



**Biodiversity and
Conservation Science**

Great Victoria Desert Fire Scar Mapping Report: 2020

Ricky van Dongen, Jaume Rusalleda Alvarez, Katherine Zdunic
and Jane Chapman

Great Victoria Desert Fire Scar Mapping
May 2020



Department of **Biodiversity,
Conservation and Attractions**

Department of Biodiversity, Conservation and Attractions
Locked Bag 104
Bentley Delivery Centre WA 6983
Phone: (08) 9219 9000
Fax: (08) 9334 0498

www.dbca.wa.gov.au

© Department of Biodiversity, Conservation and Attractions on behalf of the State of Western Australia 2020
September 2020

This work is copyright. You may download, display, print and reproduce this material in unaltered form (retaining this notice) for your personal, non-commercial use or use within your organisation. Apart from any use as permitted under the *Copyright Act 1968*, all other rights are reserved. Requests and enquiries concerning reproduction and rights should be addressed to the Department of Biodiversity, Conservation and Attractions.

This report/document/publication was prepared by Jaime Ruscallea Alvarez and Ricky van Dongen

Questions regarding the use of this material should be directed to:
Remote Sensing Research Officer
Biodiversity and conservation Science
Department of Biodiversity, Conservation and Attractions
Locked Bag 104
Bentley Delivery Centre WA 6983
Phone: 9219 9571
Email: Ricky.vandongen@dbca.wa.gov.au

The recommended reference for this publication is:
van Dongen R., Ruscallea-Alvarez J., Zdunic K. and Chapman J., 2020: *Great Victoria Desert Fire Scar Mapping Report: Final Report*, Department of Biodiversity, Conservation and Attractions, Perth.

This document is available in alternative formats on request.

Contents

Summary	vii
1 Introduction	1
2 Methodology	2
2.1 Satellite Data	2
2.2 Fire scar mapping methodology	2
2.3 Fire statistics	4
2.4 Rainfall data	4
2.5 Time series graph	4
2.6 Comparing DBCA Landsat-based and NAFI MODIS-based fire products.....	4
3 Results	5
3.1 Statistics by IBRA.....	5
3.2 Plot scale fire and recovery	24
3.3 DBCA Landsat-based and NAFI MODIS-based fire products: differences and causes	27
3.3.1 Summary	27
3.3.2 Study area	27
3.3.3 Results.....	28
3.3.4 Discussion	40
3.3.5 Conclusions	40
References.....	41
Appendix 1	42
 Appendix 1	
Image dates for 107/80	42
Image dates for 107/81	43
Image dates for 108/80	44
Image dates for 108/81	45
Image dates for 108/78	46
Image dates for 108/79	47
Image dates for 107/79	48
Image dates for 106/80	49
Image dates for 106/79	50
Image dates for 105/79	51
Image dates for 105/80	52

Figures

Figure 1: Landsat scene locations within the Great Victoria Desert.	vii
Figure 2: "Previous" and "current" landsat images. In this case 2014 and 2015 images from the Great Victoria Desert.	2
Figure 3: a) an image with pixel values showing the difference between nbr values from the current and previous images. Dark areas indicate a reduction in the nbr value. b) a segmented nbr difference image.	3
Figure 4: a) changes identified in the Landsat imagery, and b) fire manually identified from other change.	3
Figure 5: Burnt area by year for the Central IBRA subregion with annual rainfall.	6
Figure 6: Burnt area by year for the Shield IBRA subregion with annual rainfall.	7
Figure 7: Burnt area by year for the Maralinga IBRA subregion with annual rainfall. .	8
Figure 8: Burnt area by year for the Kintore IBRA subregion with annual rainfall.	9
Figure 9: Average burnt area patch size by year for all IBRA subregions.	10
Figure 10: Vegetation age classes area according to years since last burn in the Central and Shield IBRA subregions.	10
Figure 11: Proportion of vegetation age classes in each IBRA subregion (within the studied area) according to years since last burn in the Central and Shield IBRA subregions.	11
Figure 12: Frequency distribution of fire size classes in the Central IBRA subregion.	11
Figure 13: Frequency distribution of fire size classes in the Shield IBRA subregion.	12
Figure 14: Frequency distribution of fire size classes in the Maralinga IBRA subregion.	12
Figure 15: Frequency distribution of fire size classes in the Kintore IBRA subregion.	13
Figure 16: Proportion of studied area burnt in different fire size classes in the Central IBRA subregion.	13
Figure 17: Proportion of studied area burnt in different fire size classes in the Shield IBRA subregion.	14
Figure 18: Proportion of studied area burnt in different fire size classes in the Maralinga IBRA subregion.	14
Figure 19: Proportion of studied area burnt in different fire size classes in the Kintore IBRA subregion.	15
Figure 20: Fire frequency for the Shield IBRA region.	20
Figure 21: Fire frequency for the Central IBRA region.	20
Figure 22: Fire frequency for the Maralinga IBRA region.	21
Figure 23: Fire frequency for the Kintore IBRA region.	21

Figure 24: Fire interval for the Central IBRA region.....	22
Figure 25: Fire interval for the Shield IBRA region.	22
Figure 26: Fire interval for the Maralinga IBRA region.	23
Figure 27: Fire interval for the Kintore IBRA region.....	23
Figure 28: Location of time series plots.....	24
Figure 29: Time series graph of vegetation cover values for an area which did not burn in the 1995 to 2018 time period.	25
Figure 30: Time series graph of vegetation cover values for an area which burnt once in the 1995 to 2018 time period.....	25
Figure 31: Time series graph of vegetation cover values for an area which burnt twice in the 1995 to 2018 time period.	26
Figure 32: Time series graph of vegetation cover values for an area which burnt three times in the 1995 to 2018 time period.....	26
Figure 33. DBCA Landsat-based and NAFI MODIS-based fire product comparison: study area in the western sector of the Great Victoria Desert.....	28
Figure 34. Proportion of different geographical extents that appear to have burnt at least once, from 2000 to 2019, derived from DBCA Landsat-based and NAFI MODIS-based fire products. Red outlines show commission errors (within burnt) and omission errors (within unburnt) of the NAFI MODIS-based method	29
Figure 35. Annual burnt area in the West GVD Central IBRA subregion, from 2000 to 2019, derived from DBCA Landsat-based and NAFI MODIS-based fire products.	31
Figure 36. Annual burnt area in the West GVD Shield IBRA subregion, from 2000 to 2019, derived from DBCA Landsat-based and NAFI MODIS-based fire products.	31
Figure 37. Annual burnt area in the proposed fire management area, from 2000 to 2019, derived from DBCA Landsat-based and NAFI MODIS-based fire products.	32
Figure 38. Annual burnt area in the proposed fire reference area, from 2000 to 2019, derived from DBCA Landsat-based and NAFI MODIS-based fire products.	32
Figure 39. Proportion of the studied geographical extents in which there is an agreement, a difference of 1 year or a disagreement in year since last burn between DBCA Landsat-based and NAFI MODIS-based methods.	33
Figure 40. Fuel age area distribution calculated as years since last burn in the West GVD Central IBRA bioregion, from 2000 to 2019, derived from DBCA Landsat-based and NAFI MODIS-based fire products.....	35
Figure 41. Fuel age area distribution calculated as years since last burn in the West GVD Shield IBRA bioregion, from 2000 to 2019, DBCA Landsat-based and NAFI MODIS-based fire products.....	35
Figure 42. Fuel age area distribution calculated as years since last burn in the proposed fire management area, from 2000 to 2019, DBCA Landsat-based and NAFI MODIS-based fire products.	36

Figure 43. Fuel age area distribution calculated as years since last burn in the proposed fire reference area, from 2000 to 2019, DBCA Landsat-based and NAFI MODIS-based fire products.....	36
Figure 44. Fuel age spatial distribution calculated as years since last burn in the proposed fire management and reference areas, from 2000 to 2019, DBCA Landsat-based and NAFI MODIS-based fire products.....	37
Figure 45. Fuel age simulation on 5 randomly located points within the fire management area, using DBCA Landsat-based and NAFI MODIS-based fire products.	37
Figure 46. Fire scar overlap and intersections between DBCA Landsat-based and NAFI MODIS-based fire products across different areas of the West GVD in 2008 (A), 2017 (B,C) and 2018 (D,E and F).....	39

Tables

Table 1: Mean, median, minimum and maximum fire areas in the Central IBRA subregion.	16
Table 2: Mean, median, minimum and maximum fire areas in the Shield IBRA subregion.	17
Table 3: Mean, median, minimum and maximum fire areas in the Maralinga IBRA subregion.	18
Table 4: Mean, median, minimum and maximum fire areas in the Kintore IBRA subregion.	19
Table 5. Number of hectares and proportion of each studied extent corresponding to the NAFI MODIS-based commission and omission errors.....	29
Table 6. Number of hectares and percentages of the studied geographical extents in which there is an agreement, a difference of 1 year or a disagreement in year since last burn (YSLB) between DBCA Landsat-based and NAFI MODIS-based methods.	34

Summary

This report provides statistics relating to fire mapping within the Great Victoria Desert (GVD) being carried out by the Department of Biodiversity, Conservation and Attractions. The report and associated datasets have been completed in accordance with Final Report requirements as specified in the scope of work for the Landsat Fire scar mapping Project – GVD-P-19-001.

The statistics provided relate to fires mapped within Landsat scenes 105/79 to 80, 106/79 to 80, 107/79 to 81, and 108/78 to 81 (Figure 1) for the GVD for the years 1995 to 2019 (inclusive).

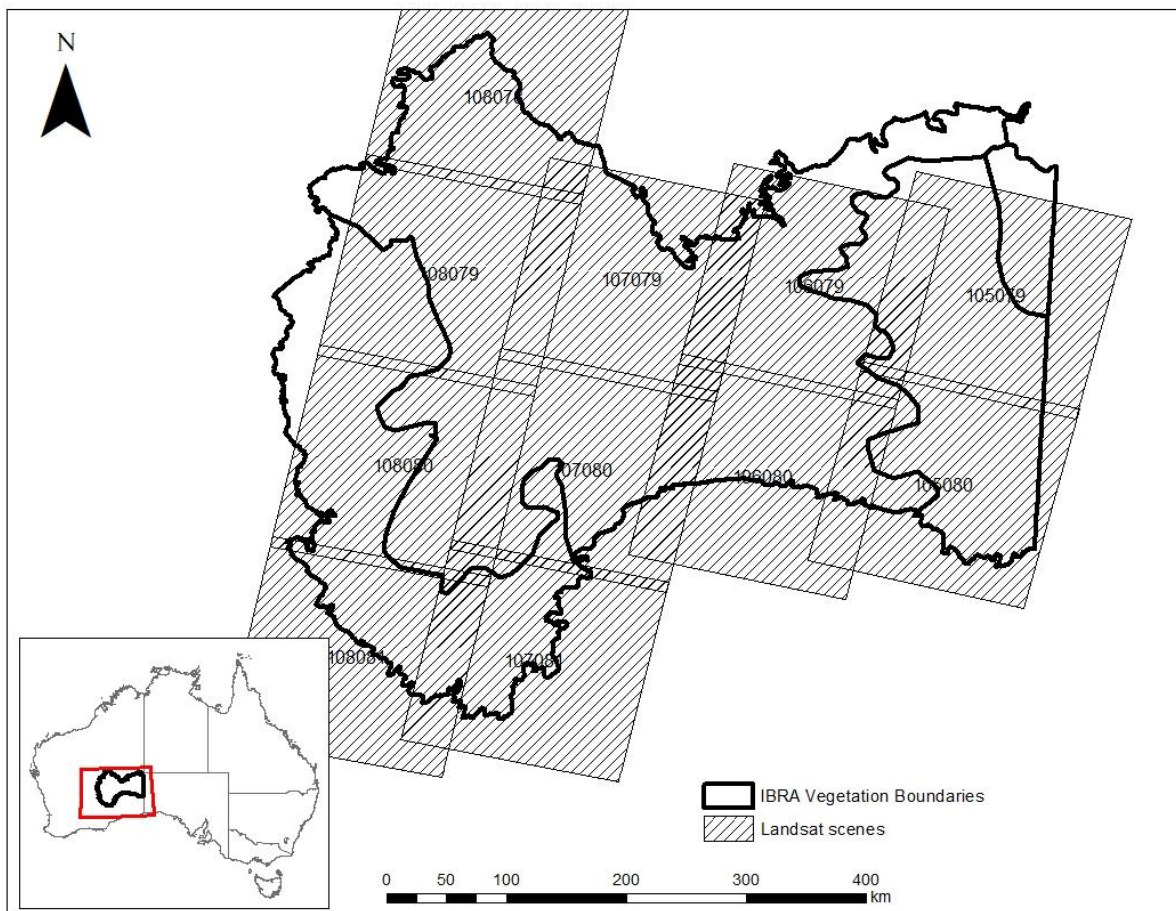


Figure 1: Landsat scene locations within the Great Victoria Desert IBRA bioregion (Interim Biogeographic Regionalisation for Australia, Tackway and Cresswell, 1995).

1 Introduction

The purpose of the project is to provide a comprehensive fire scar history for the GVD for the years 1995 to 2019 (inclusive) using Landsat satellite imagery. Landsat imagery has a ground pixel resolution of 30 metres, has been captured at regular intervals since 1988 and is available free for download from the United States Geological Survey (<https://glovis.usgs.gov/app>). Fire scar maps derived from the Landsat data allow a number of statistics to be calculated including:

1. Average burnt patch size for each year of the study period;
2. Identify areas of 'long unburnt' vegetation. For the purpose of the study, 'long unburnt' will be classified as unburnt for the duration of the study; and
3. Determine the average interval of return between fires.

Currently the only fire scar maps available over the Western Australian area of the GVD are derived from MODIS satellite data and provided from the Northern Australian Fire Information (NAFI) service (<https://www.firenorth.org.au/nafi3/>). This data is useful for regional statistics however it is based on a ground pixel resolution of 250 metres which leads to inaccuracies and omission errors. These inaccuracies and omissions are likely to have a significant impact on the validity of habitat modelling and mapping which rely on fire history as a core dataset. This includes habitat modelling for species such as Sandhill Dunnarts and Malleefowl, for which long unburnt vegetation makes up a key component of their habitat.

2 Methodology

2.1 Satellite Data

The Landsat series of satellites captures imagery at 30 m resolution across several spectral bands, of which six were used for this study (red, green, blue, near infrared, short-wave infrared 1 and short-wave infrared 2). The satellites began capturing data in 1972 with the Landsat 1 satellite (at 60 m pixel resolution) with regular captures from 1987 (at 30 m pixel resolution). The archive of Landsat imagery is available for download, free of charge, from the United State Geological Survey. For each scene location one Landsat scene per year was downloaded. Images used in the analysis are shown in the appendix.

2.2 Fire scar mapping methodology

Fire mapping was carried out using a methodology developed by DBCA using the eCognition software program (Trimble eCognition developer version 9.5). For each year's fire mapping, imagery for the current and previous years are loaded in the program. Examples of previous and current images are shown in Figure 2. Several fire scars are visible in both images however a "new" fire scar is visible on the right side of image b).

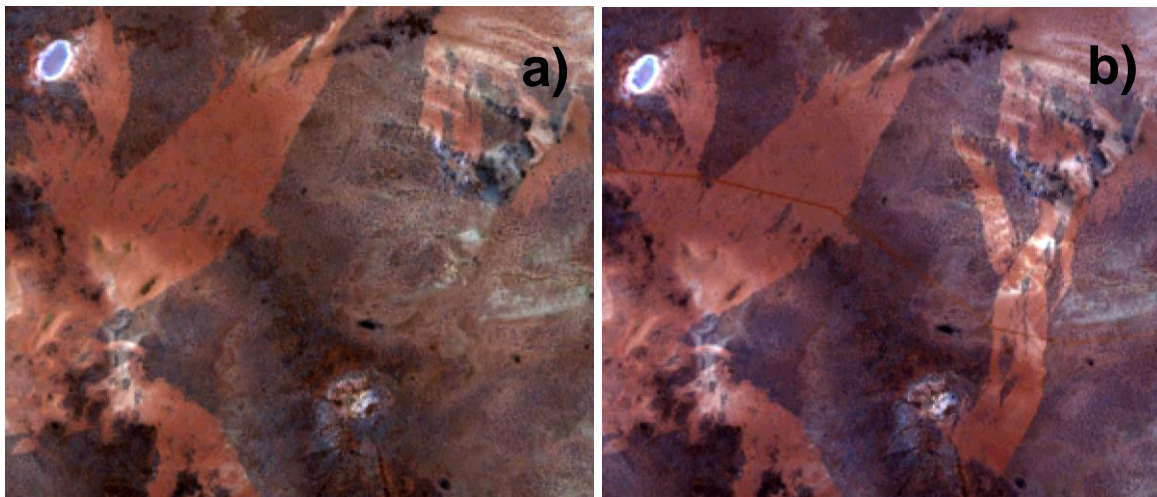


Figure 2: "Previous" and "current" landsat images. In this case 2014 and 2015 images from the Great Victoria Desert.

Difference images using the normalised burn ratio (NBR, Key and Benson 1999) and near infrared (referred to as band 4 in Landsat) for the current and previous images are created (Figure 3a). These difference images are then used in the image segmentation (Kettig and Landgrebe, 1976). The segmentation process groups pixels with similar values into segments (Figure 3b).

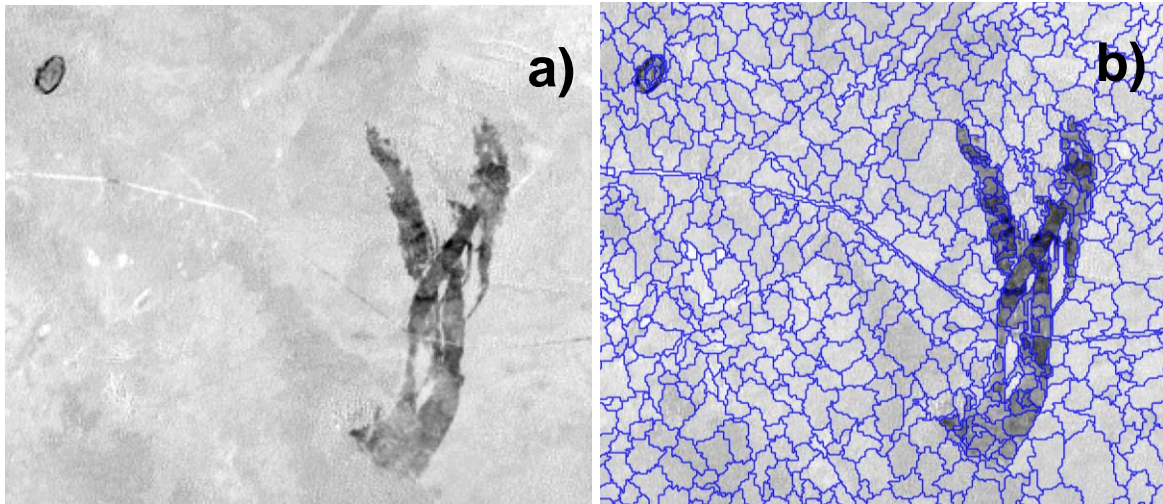


Figure 3: a) an image with pixel values showing the difference between NBR values from the current and previous images. Dark areas indicate a reduction in the NBR value. b) a segmented NBR difference image.

The mean NBR (or in some cases band 4) difference value per segment is then used to classify areas of change. A threshold value is manually set for each fire by a user. The areas of change will include fire scars and other changes, such as changes in waterbodies (Figure 4a). Fire scars are then manually identified from the areas of change and selected (Figure 4b). The selected fire scars are then exported from eCognition as an ESRI shapefile.

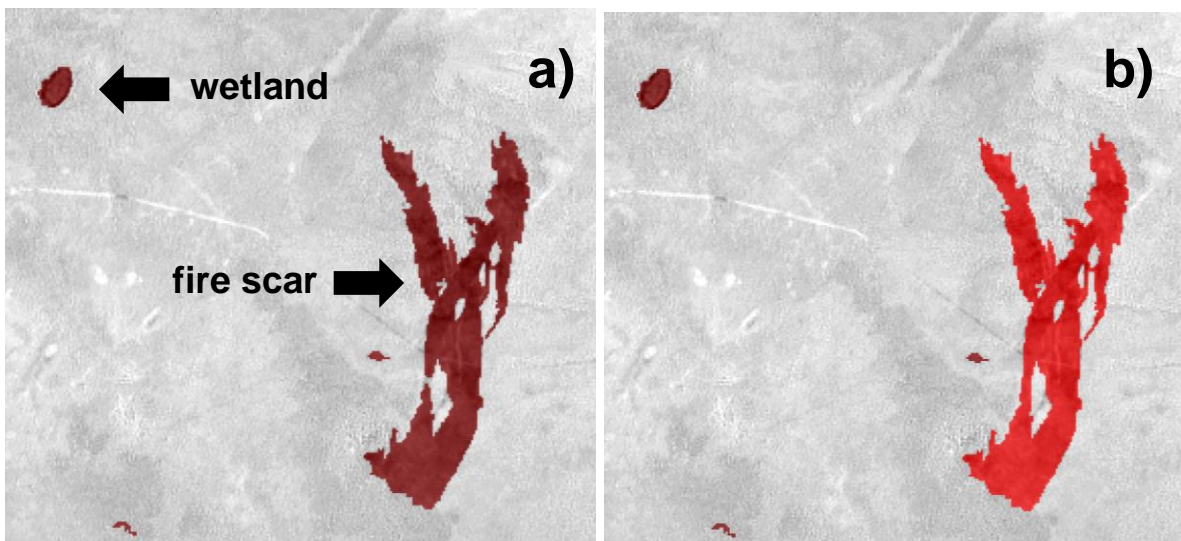


Figure 4: a) changes identified in the Landsat imagery, and b) fire manually identified from other change.

Fire attributes, such as the images used, date and year of fire are then added to the fire scar shapefile.

2.3 Fire statistics

All statistics were calculated in the R statistical environment (R version 3.6.0). Statistics have been split by IBRA region (Shield, Central, Maralinga and Kintore) and are restricted to the area of each IBRA region that overlaps with the Landsat scenes shown in Figure 1. Statistics calculated include:

- The burnt area by year for each IBRA region with average annual rainfall across each region.
- Average burnt patch size for each IBRA region.
- Years since last burn for each IBRA region.
- Proportion of vegetation age classes according to years since last burn.
- Frequency distribution of fire size classes.
- Proportion of studied area burnt in different fire size classes.
- Mean, median, minimum and maximum fire areas.
- Fire frequency for each IBRA region.
- Fire interval for each IBRA region.

2.4 Rainfall data

Rainfall data was derived from a 5 km x 5 km resolution gridded spatial dataset developed through interpolation of historical data from climate stations throughout Australia and produced in the context of the Australian Water Availability Project (AWAP, <http://www.bom.gov.au/jsp/awap/>). Available rainfall data was available until May of 2019, so annual averages presented in this report cover the period 1995-2018.

2.5 Time series graph

Time series graphs for area with a range of fire frequencies were created by extracting i35 index values from all available Landsat images. The index values were then converted to vegetation cover by regressing vegetation cover estimated from aerial photography against the index values (Zdunic and Huntley, 2015).

2.6 Comparing DBCA Landsat-based and NAFI MODIS-based fire products

A comparative study was carried out to detect and quantify differences between NAFI MODIS-based fire products (freely available from <https://www.firenorth.org.au/nafi3/>) and DBCA Landsat-based fire products generated in this study. The western sector of the GVD was chosen to perform this analysis and compared fire statistics are reported across the following geographical extents: Central IBRA subregion within the study area, Shield IBRA subregion extent within the study area, proposed fire management area and proposed reference area. Fire statistics reported include:

- Burnt area
- Year since last burn
- Fire scar

A short discussion is also included suggesting possible causes of the observed differences between both methods, as well as conclusions highlighting some of each products' optimal applications.

3 Results

3.1 Statistics by IBRA

The figures and tables shown below include statistics from fire mapping using Landsat imagery in the GVD (see Figure 1) for the time period 1995 to 2019.

- The burnt area by year for each IBRA region with annual rainfall area – Figures 5 to 8;
- Average burnt patch size for each IBRA region - Figure 9;
- Years since last burn for each IBRA region -Figure 10;
- Proportion of vegetation age classes according to years since last burn - Figure 11;
- Frequency distribution of fire size classes – Figures 12 to 15 ;
- Proportion of studied area burnt in different fire size classes – Figures 16 to 19;
- Mean, median, minimum and maximum fire areas – Tables 1 to 4;
- Fire frequency for each IBRA region - 20 to 23; and
- Fire interval for each IBRA region – Figures 24 to 27.

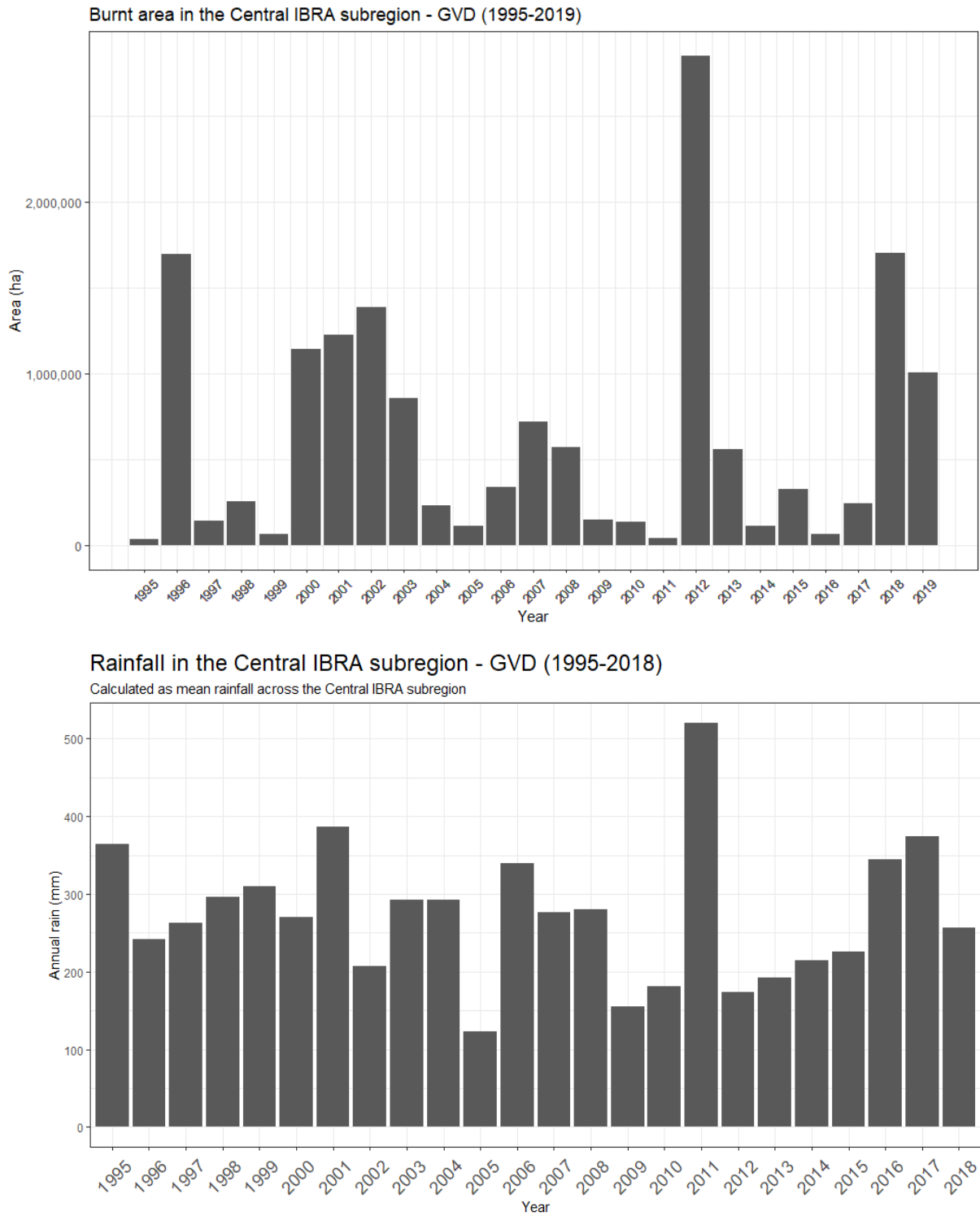


Figure 5: Burnt area by year for the Central IBRA subregion with annual rainfall.

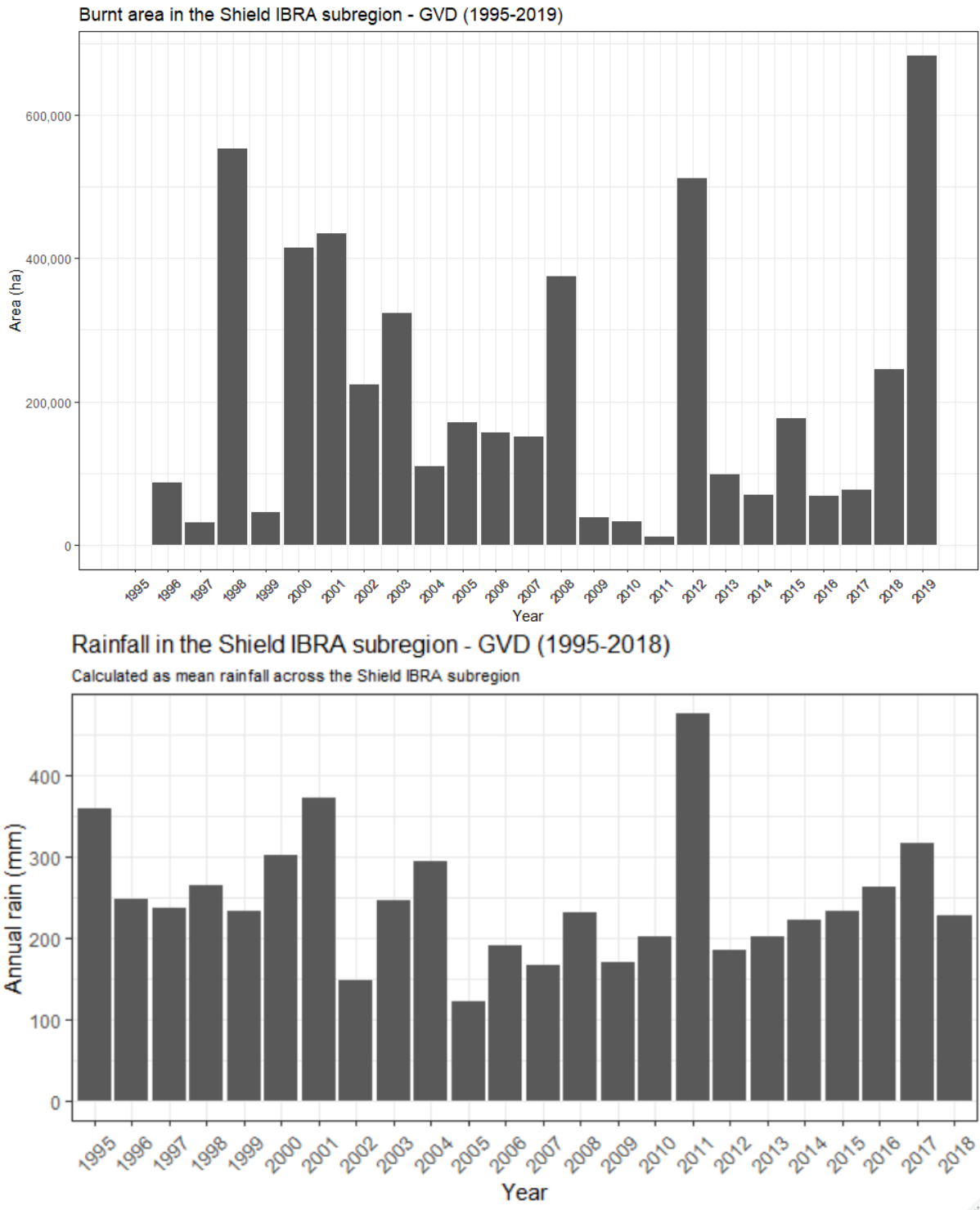


Figure 6: Burnt area by year for the Shield IBRA subregion with annual rainfall.

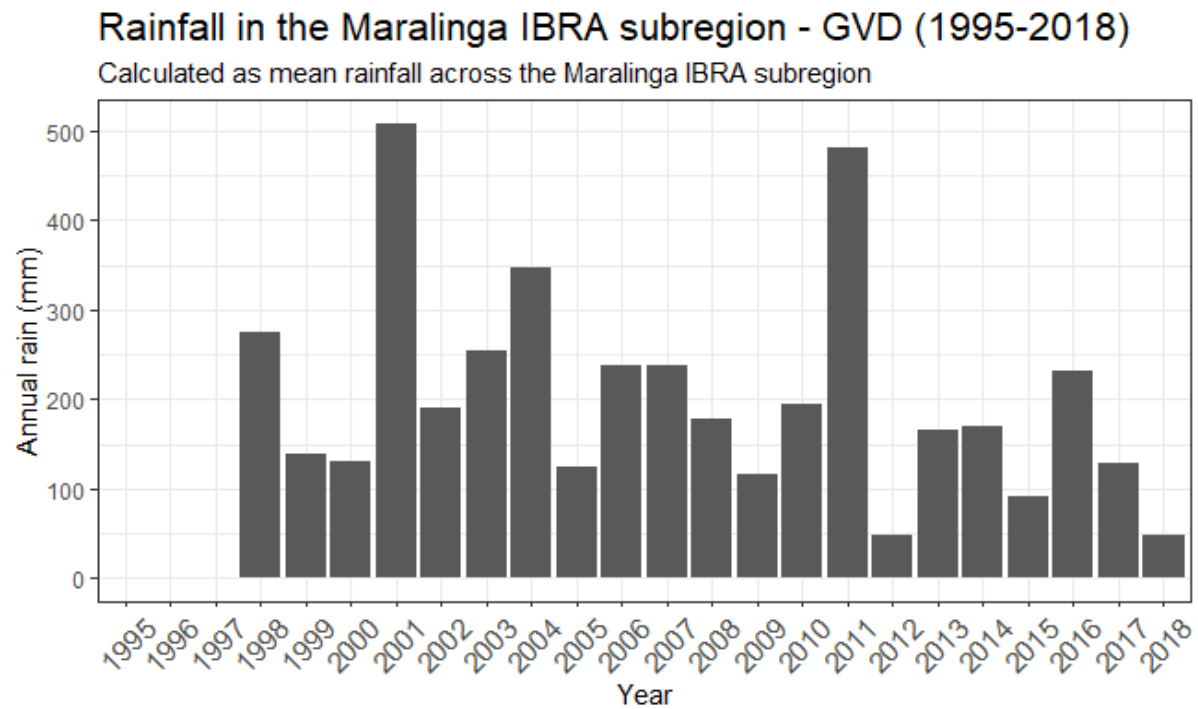
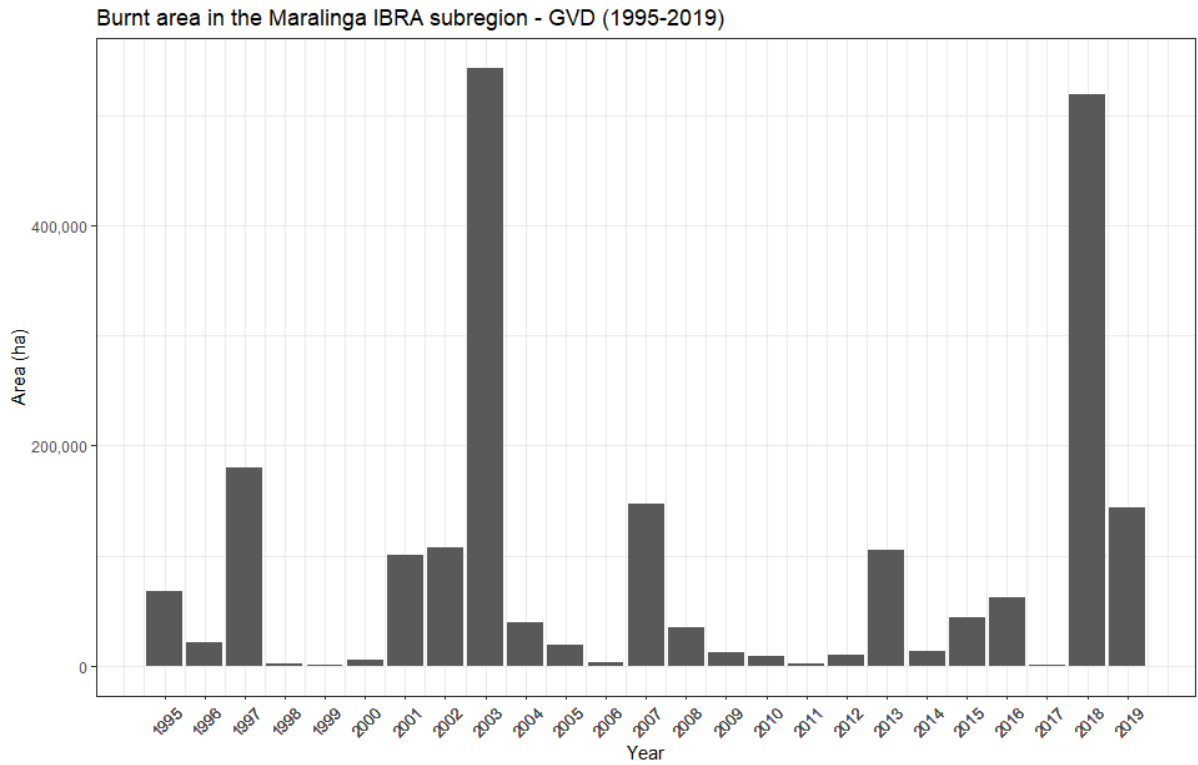
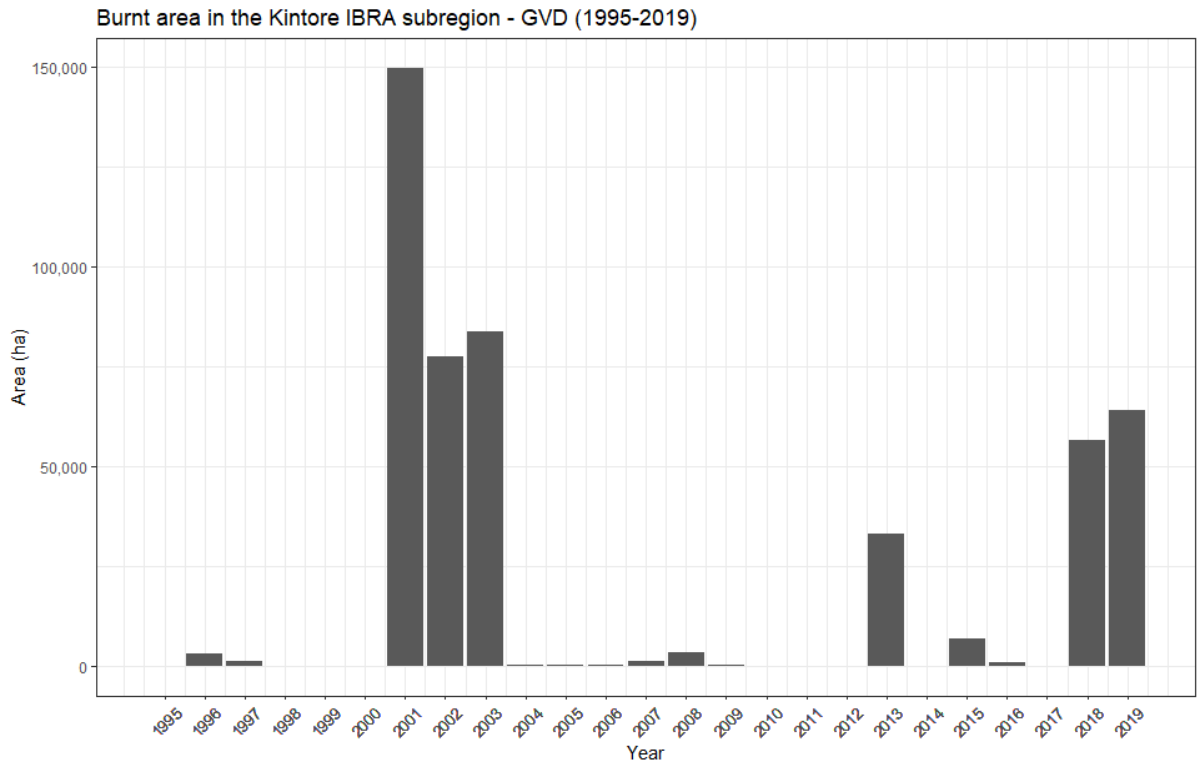


Figure 7: Burnt area by year for the Maralinga IBRA subregion with annual rainfall. 1995, 1996 and 1997 are real 0's or very low values.



Rainfall in the Kintore IBRA subregion - GVD (1995-2018)

Due to many years of missing data in the Kintore subregion, calculated as mean rainfall across the adjacent Maralinga IBRA subregion

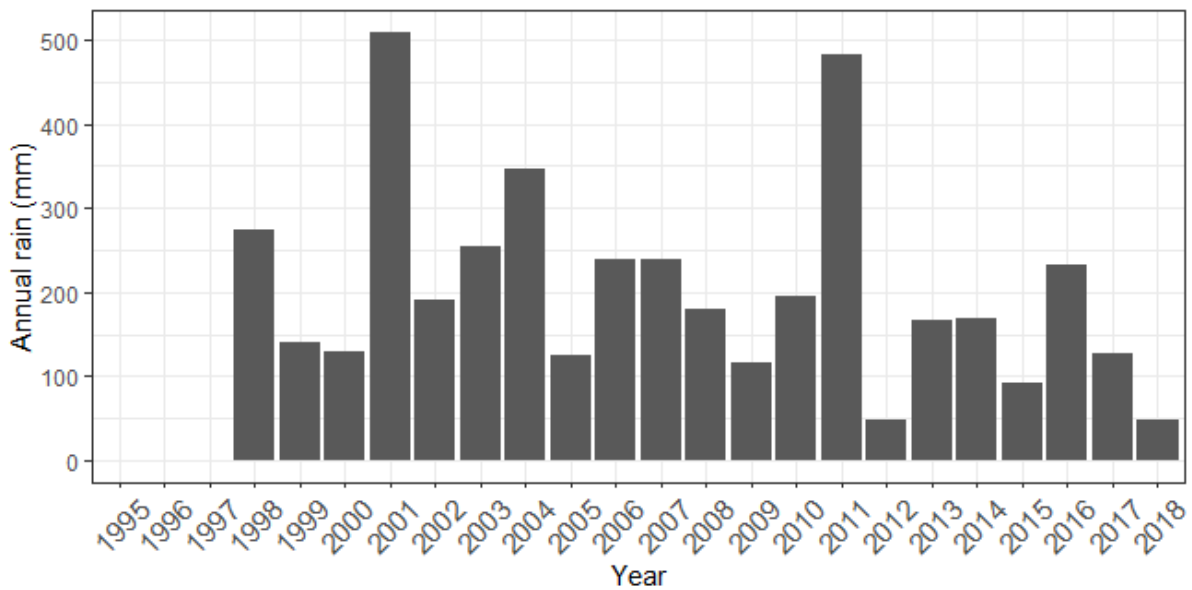


Figure 8: Burnt area by year for the Kintore IBRA subregion with annual rainfall. 1995, 1996 and 1997 are real 0's or very low values.

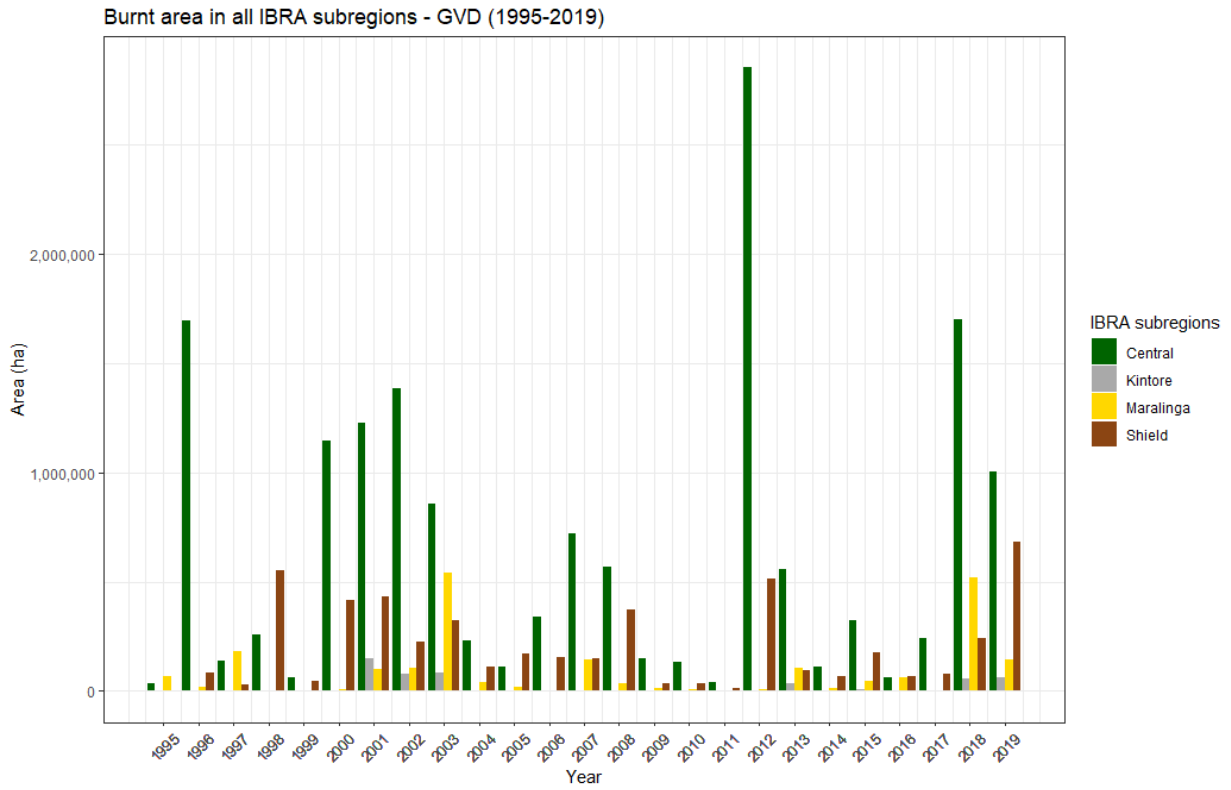


Figure 9: Average burnt area patch size by year for all IBRA subregions.

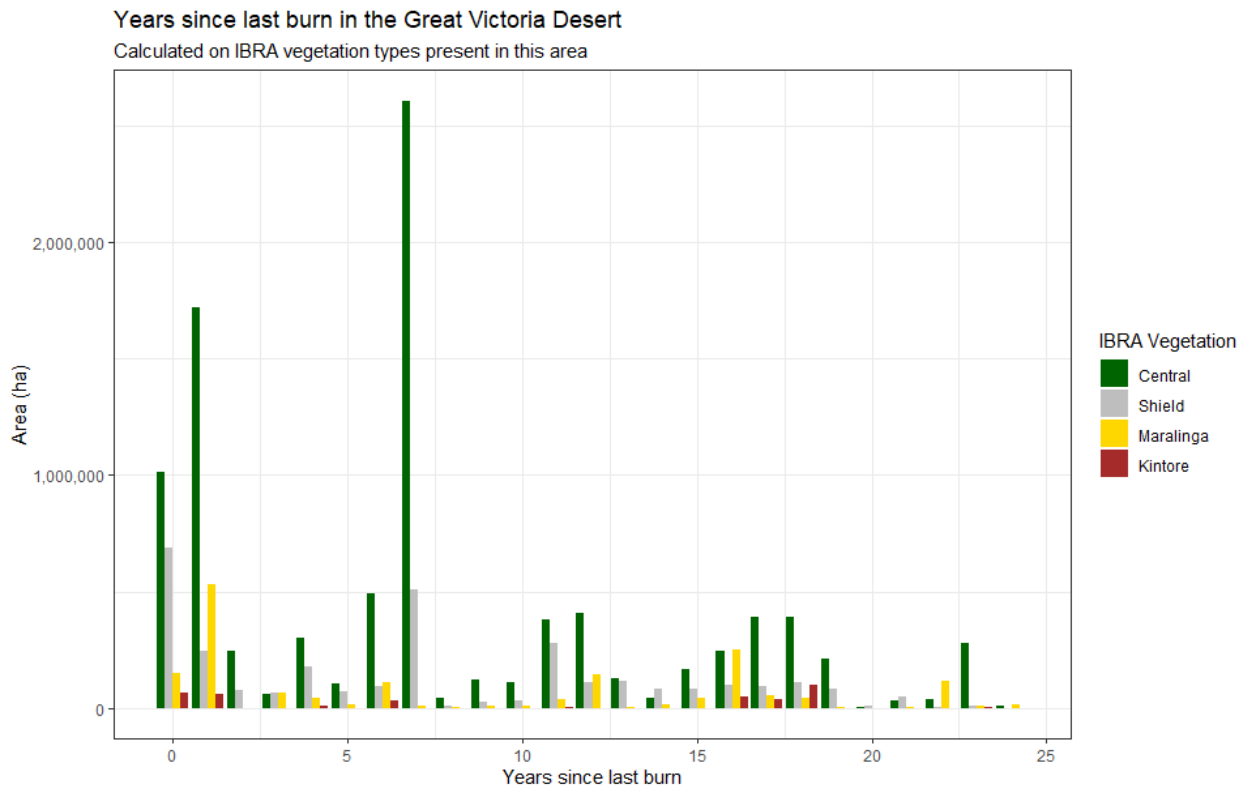


Figure 10: Vegetation age classes area according to years since last burn in the Central and Shield IBRA subregions.

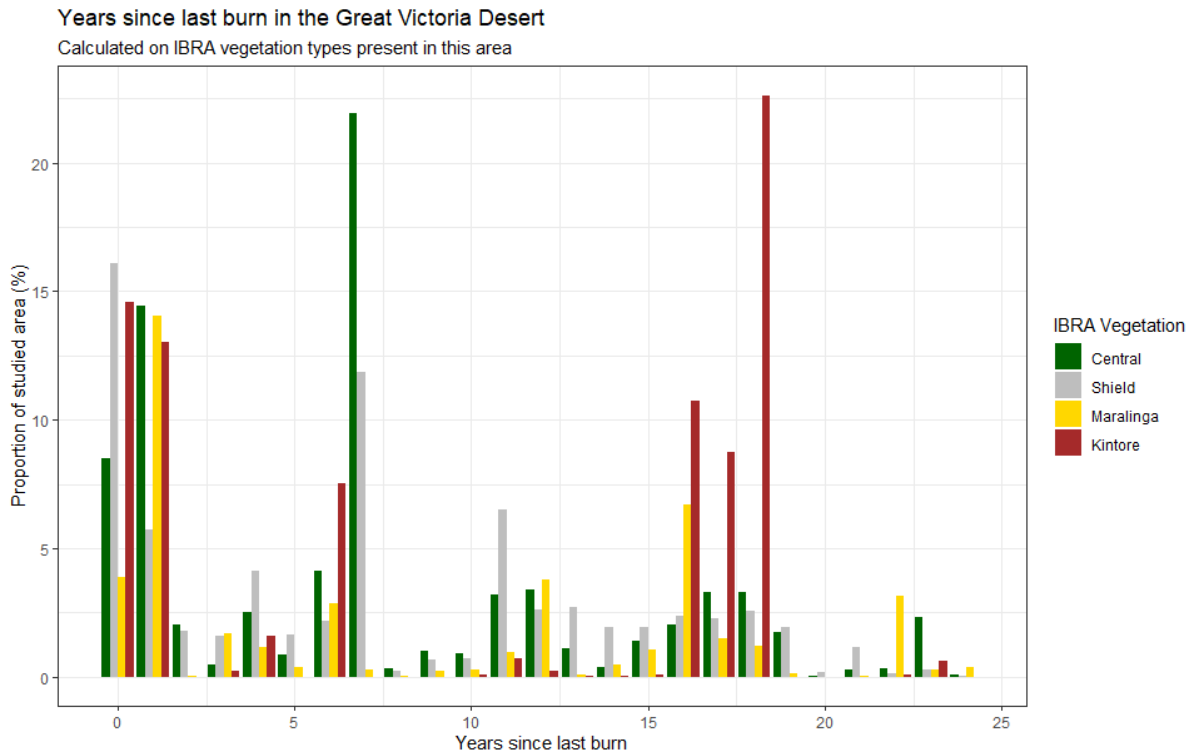


Figure 11: Proportion of vegetation age classes in each IBRA subregion (within the studied area) according to years since last burn in the Central and Shield IBRA subregions

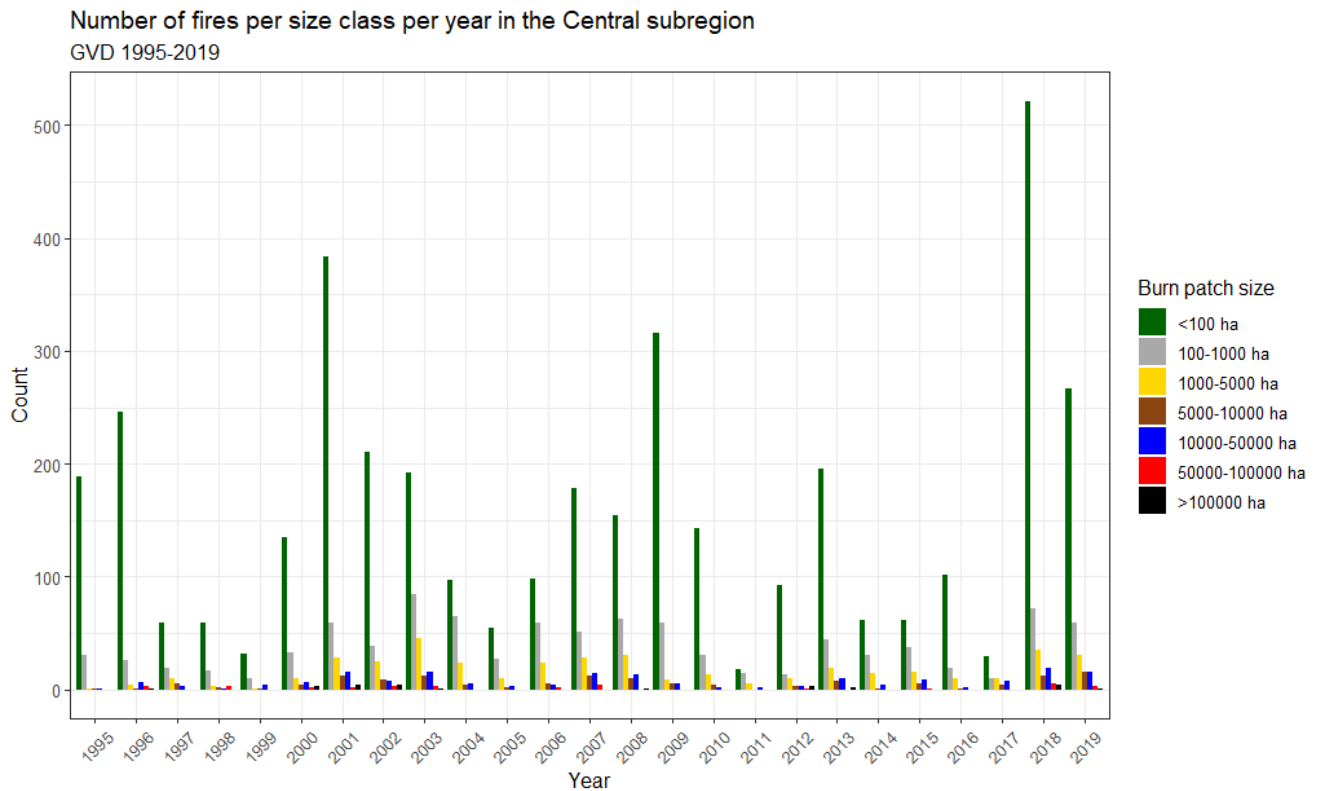


Figure 12: Frequency distribution of fire size classes in the Central IBRA subregion.

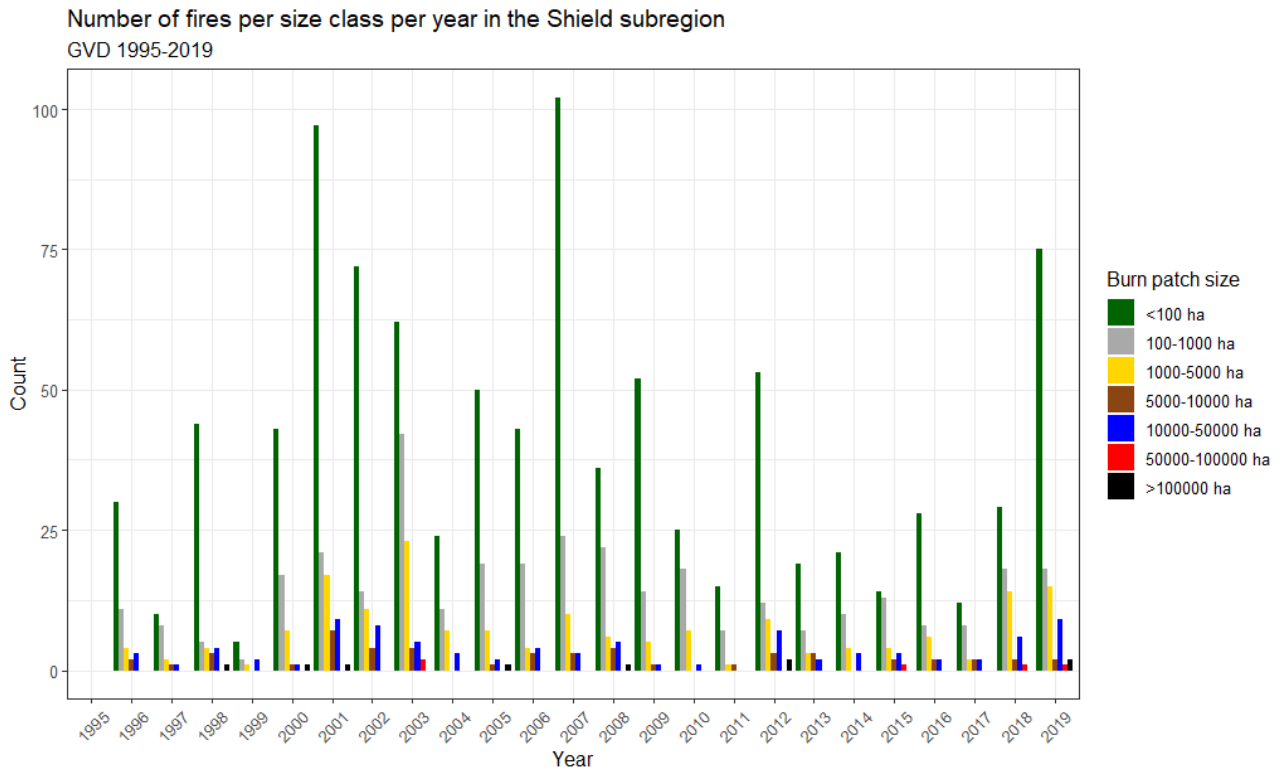


Figure 13: Frequency distribution of fire size classes in the Shield IBRA subregion.

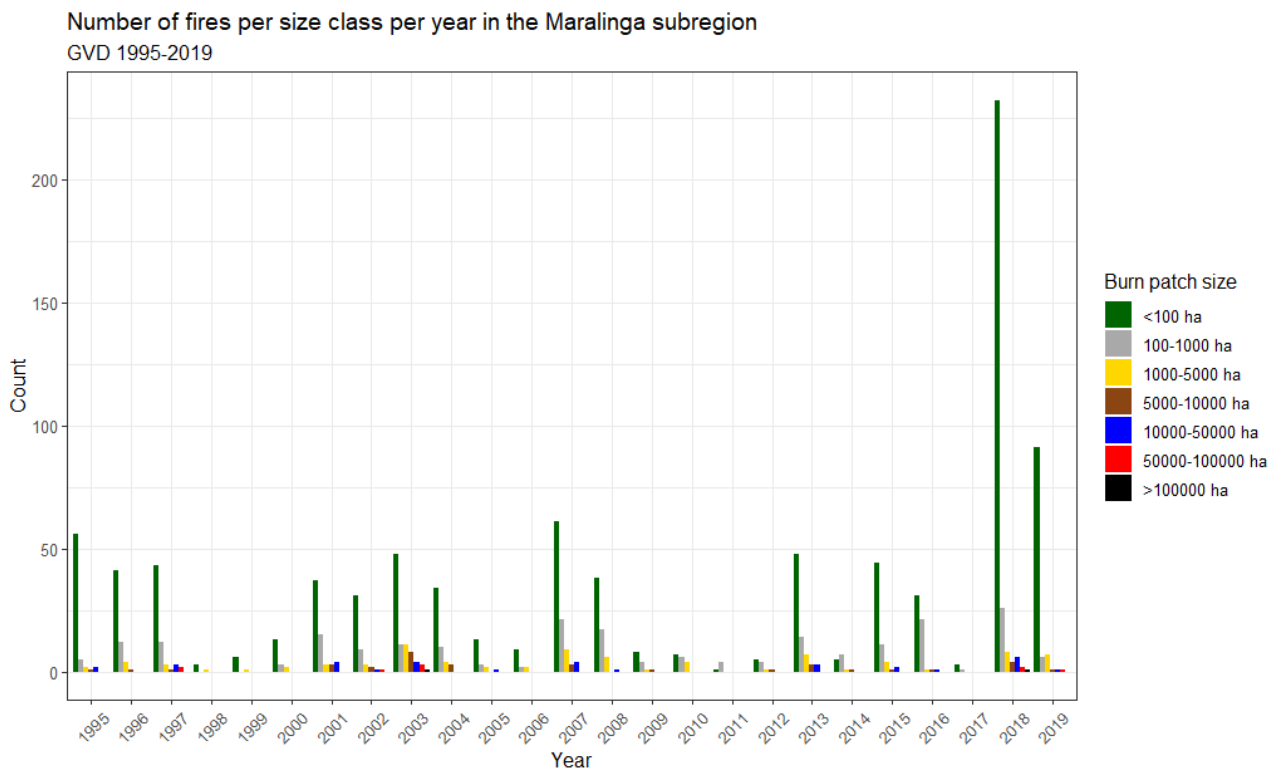


Figure 14: Frequency distribution of fire size classes in the Maralinga IBRA subregion.

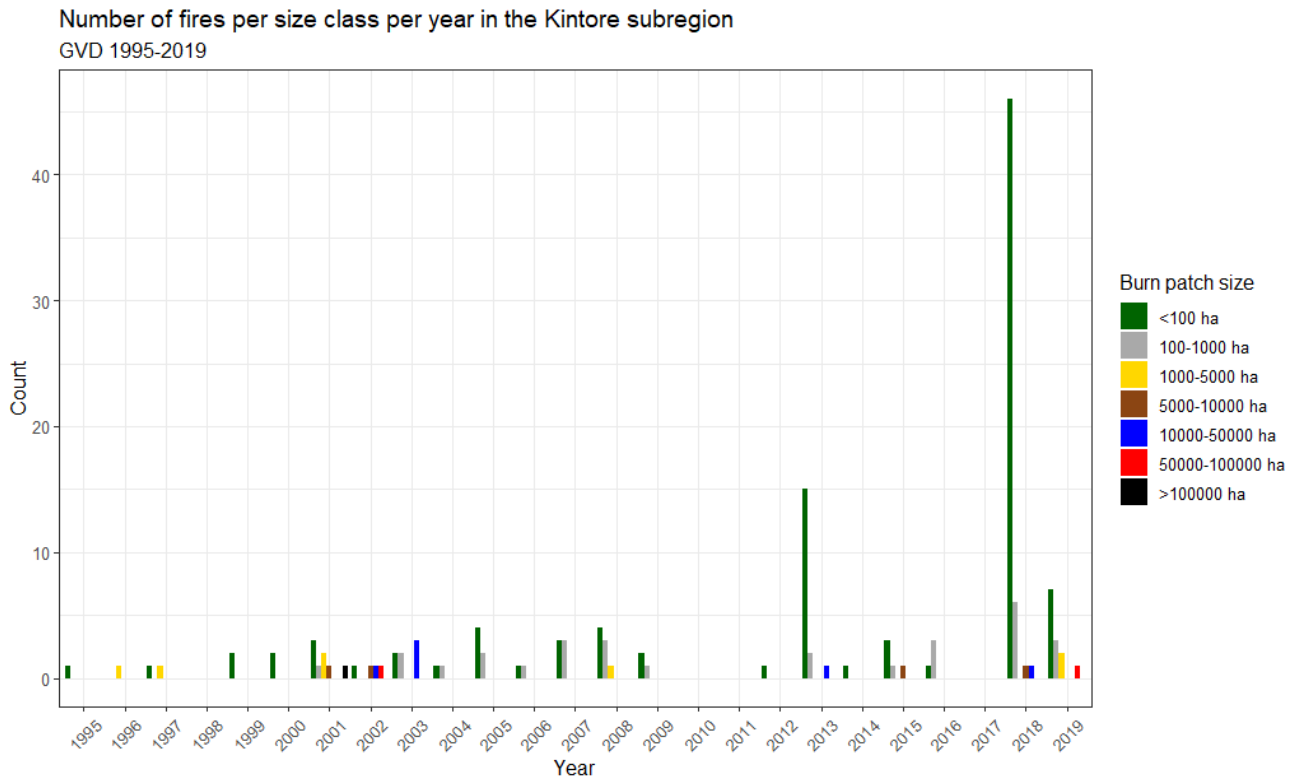


Figure 15: Frequency distribution of fire size classes in the Kintore IBRA subregion.

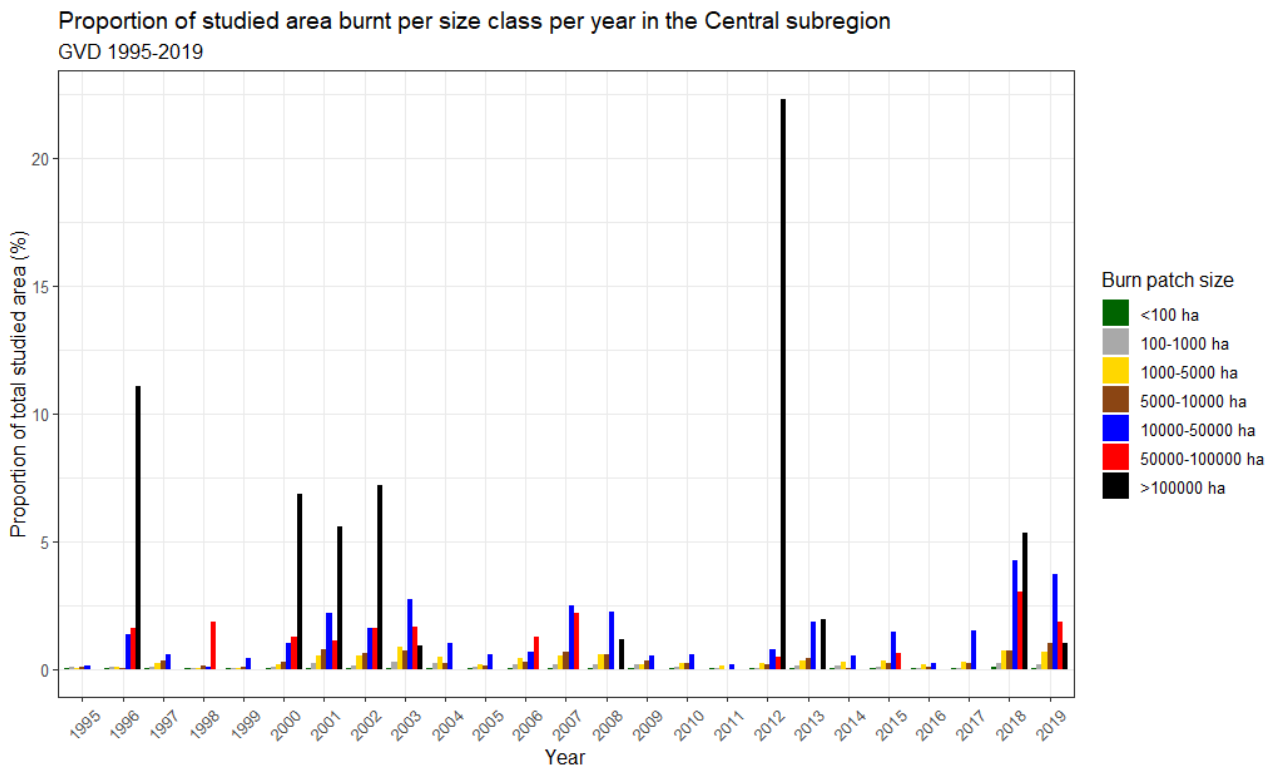


Figure 16: Proportion of studied area burnt in different fire size classes in the Central IBRA subregion.

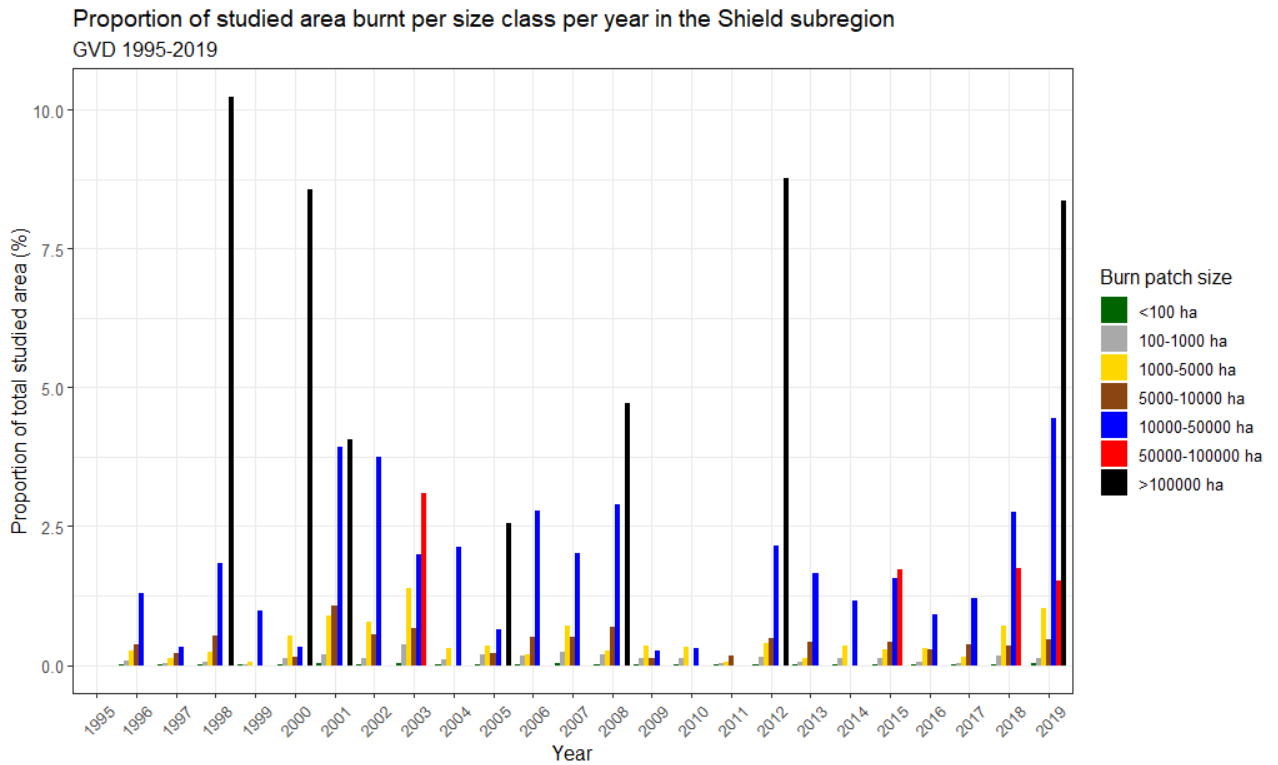


Figure 17: Proportion of studied area burnt in different fire size classes in the Shield IBRA subregion.

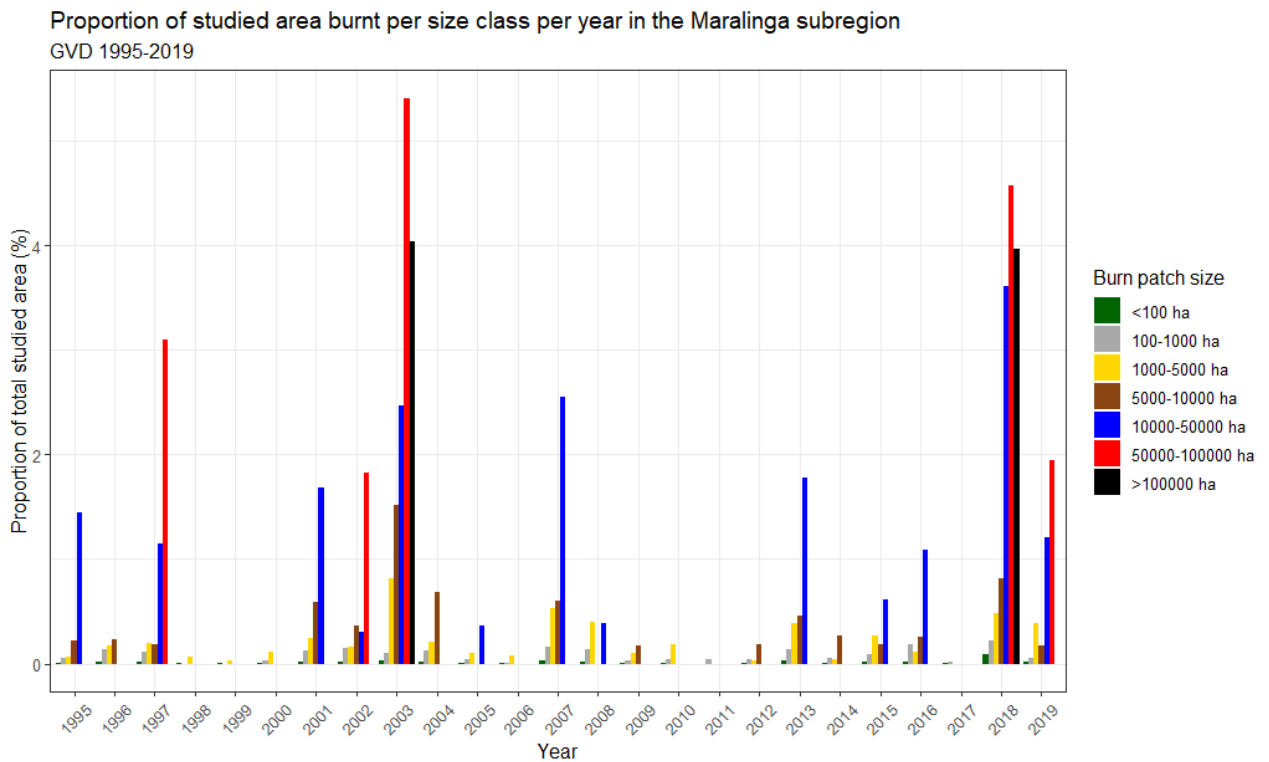


Figure 18: Proportion of studied area burnt in different fire size classes in the Maralinga IBRA subregion.

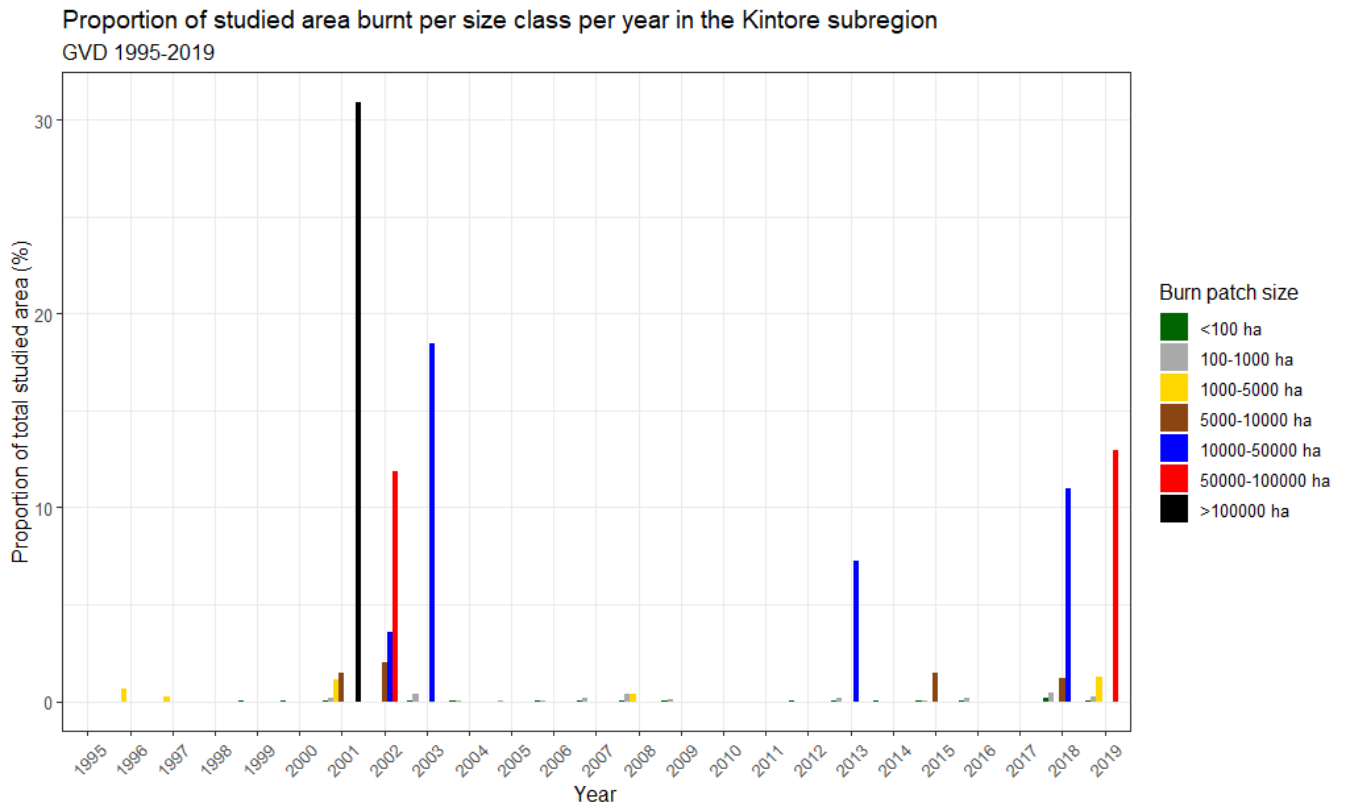


Figure 19: Proportion of studied area burnt in different fire size classes in the Kintore IBRA subregion.

Fire metrics for the Central IBRA subregion

GVD (1995-2019)

Year	Mean (ha)	Median (ha)	Min (ha)	Max (ha)
1995	164	7.5	0.36	14182
1996	5912	5.4	0.36	1314119
1997	1455	62.4	0.36	41142
1998	3013	34.5	0.36	82594
1999	1319	62.4	0.99	14160
2000	5932	20.8	0.45	492558
2001	2438	9.5	0.36	223010
2002	4671	17.8	0.45	324949
2003	2428	61.8	0.36	110810
2004	1175	102.8	0.45	43617
2005	1168	68.5	0.66	31775
2006	1758	90.2	0.45	85850
2007	2513	33.2	0.45	71102
2008	2096	53.4	0.45	136357
2009	381	10.3	0.54	19616
2010	703	17.7	0.63	42538
2011	1106	125.7	3.87	12592
2012	22814	7.7	0.36	2274086
2013	2010	12.7	0.36	127116
2014	1003	69.9	0.54	20152
2015	2541	105.7	0.81	74108
2016	482	18.8	0.36	13275
2017	4045	121.6	0.45	40217
2018	2547	8.3	0.36	173239
2019	2564	13.9	0.45	122054

Table 1: Mean, median, minimum and maximum burnt patch size in the Central IBRA subregion.

Fire metrics for the Shield IBRA subregion GVD (1995-2019)

Year	Mean (ha)	Median (ha)	Min (ha)	Max (ha)
1995	0	0.0	0.00	0
1996	1725	21.7	0.72	25331
1997	1391	120.9	5.76	13906
1998	9066	5.7	0.36	437556
1999	4527	123.4	1.46	29895
2000	5927	20.3	0.36	366172
2001	2862	20.4	0.36	173642
2002	2057	17.6	0.36	40037
2003	2341	146.6	0.36	77193
2004	2446	89.9	0.54	42337
2005	2138	34.8	0.36	109704
2006	2150	29.0	0.90	36960
2007	1059	15.6	0.36	30471
2008	5061	119.9	0.86	201933
2009	516	11.8	0.58	11379
2010	638	107.4	0.99	12681
2011	469	61.4	1.08	7331
2012	5956	19.3	0.36	205707
2013	2874	52.6	0.36	43332
2014	1835	69.2	0.36	25654
2015	4759	248.7	1.26	73600
2016	1477	71.9	0.82	25337
2017	2936	106.4	2.07	29689
2018	3493	239.2	0.81	74482
2019	5598	31.9	0.36	185883

Table 2: Mean, median, minimum and maximum burnt patch size in the Shield IBRA subregion.

Fire metrics for the Maralinga IBRA subregion

GVD (1995-2019)

Year	Mean (ha)	Median (ha)	Min (ha)	Max (ha)
1995	1030	2.5	0.36	28668
1996	358	17.3	1.62	8583
1997	2808	25.1	0.36	63100
1998	628	24.6	0.72	2461
1999	196	22.0	7.75	1230
2000	312	21.0	5.99	2701
2001	1629	32.6	1.76	23621
2002	2275	42.6	1.17	69022
2003	6308	53.2	0.76	152282
2004	768	34.8	2.07	9875
2005	1014	30.0	1.26	13864
2006	264	22.2	3.51	1931
2007	1497	28.8	0.45	31527
2008	571	38.9	0.36	14470
2009	842	67.7	0.56	6500
2010	504	147.3	1.62	2224
2011	340	162.8	8.29	765
2012	918	119.2	0.36	7161
2013	1402	27.2	0.36	32538
2014	985	171.0	1.08	9962
2015	715	20.6	0.45	12123
2016	1131	59.5	1.17	40946
2017	159	33.1	3.87	567
2018	1861	6.8	0.36	149712
2019	1340	5.5	0.36	73590

Table 3: Mean, median, minimum and maximum burnt patch size in the Maralinga IBRA subregion.

Fire metrics for the Kintore IBRA subregion GVD (1995-2019)

Year	Mean (ha)	Median (ha)	Min (ha)	Max (ha)
1995	7	6.9	6.94	7
1996	2958	2958.0	2958.01	2958
1997	580	579.5	5.04	1154
1998	0	0.0	0.00	0
1999	12	11.8	11.26	12
2000	9	8.5	7.34	10
2001	18697	1106.9	3.74	137025
2002	19335	12312.3	2.75	52711
2003	11964	906.5	12.93	35199
2004	169	169.4	44.54	294
2005	44	3.5	3.12	131
2006	121	120.9	87.84	154
2007	180	117.4	31.03	510
2008	404	162.3	0.42	1624
2009	117	14.3	5.94	331
2010	0	0.0	0.00	0
2011	0	0.0	0.00	0
2012	42	41.7	41.70	42
2013	1835	8.6	1.35	32155
2014	20	20.4	20.45	20
2015	1328	57.0	6.44	6390
2016	234	251.4	44.99	387
2017	0	0.0	0.00	0
2018	1048	6.7	0.72	48595
2019	4924	75.5	1.17	57329

Table 4: Mean, median, minimum and maximum burnt patch size in the Kintore IBRA subregion.

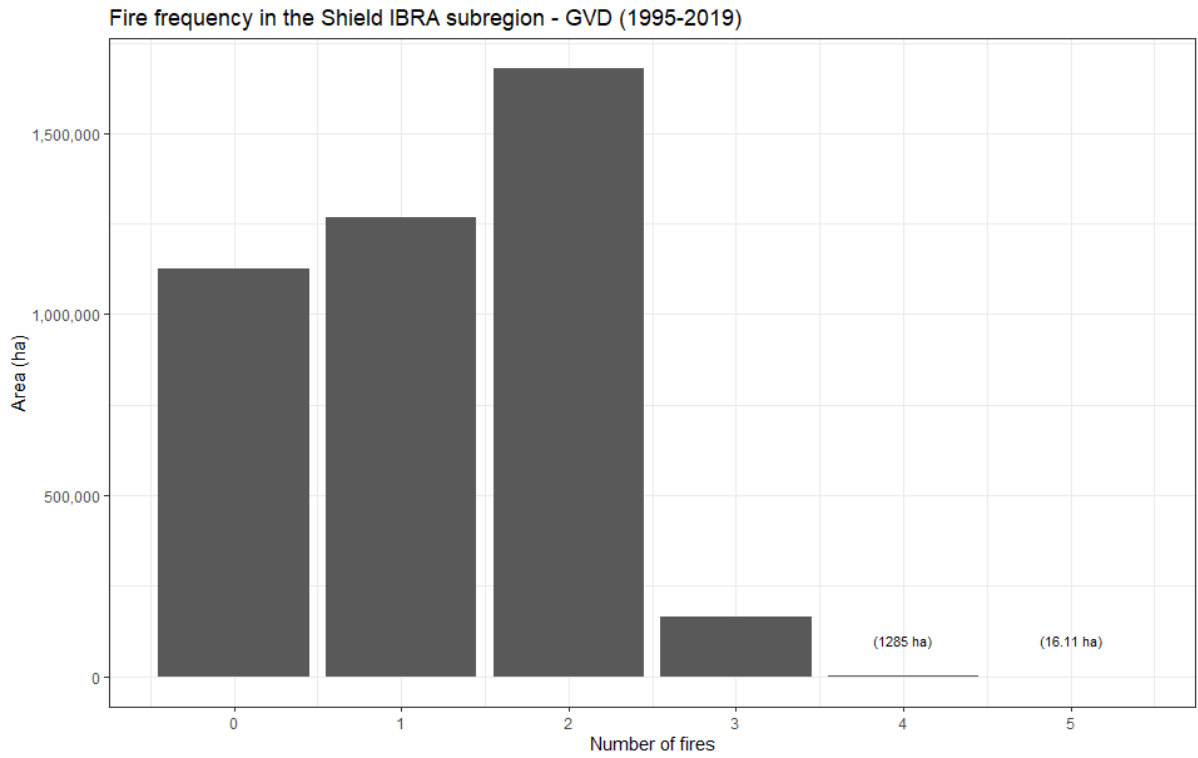


Figure 20: Fire frequency for the Shield IBRA region.

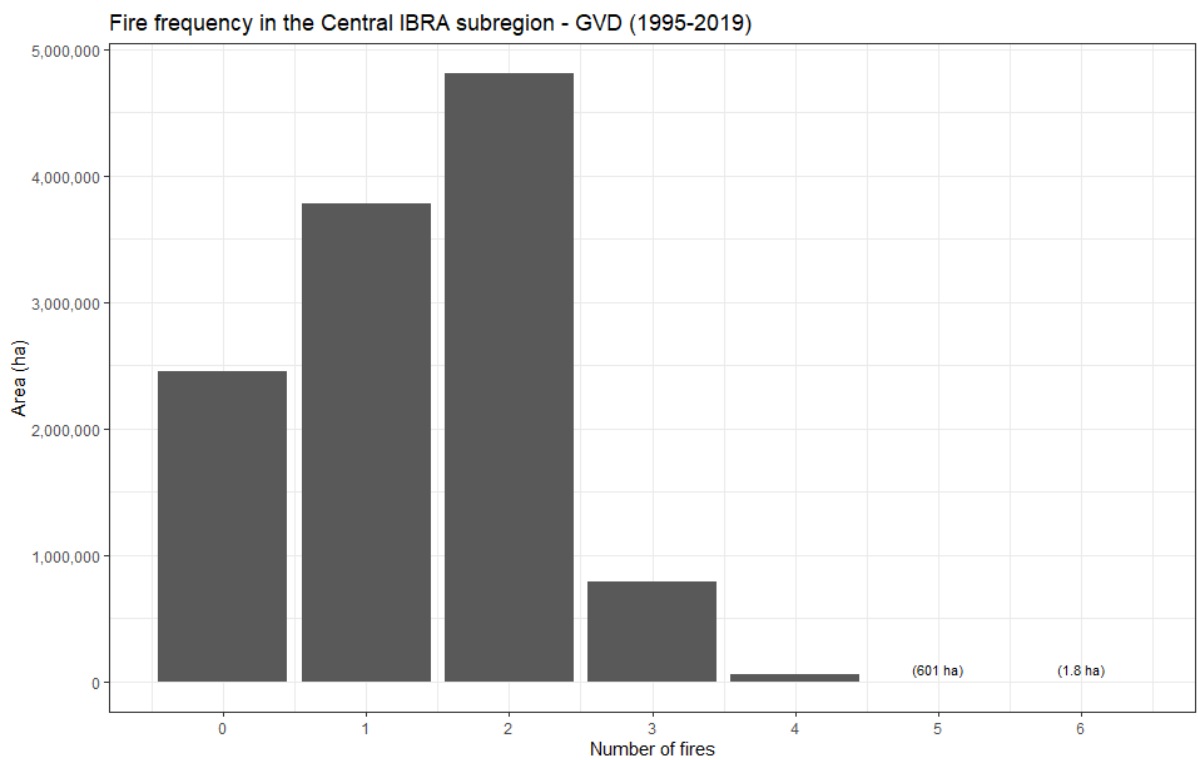


Figure 21: Fire frequency for the Central IBRA region.

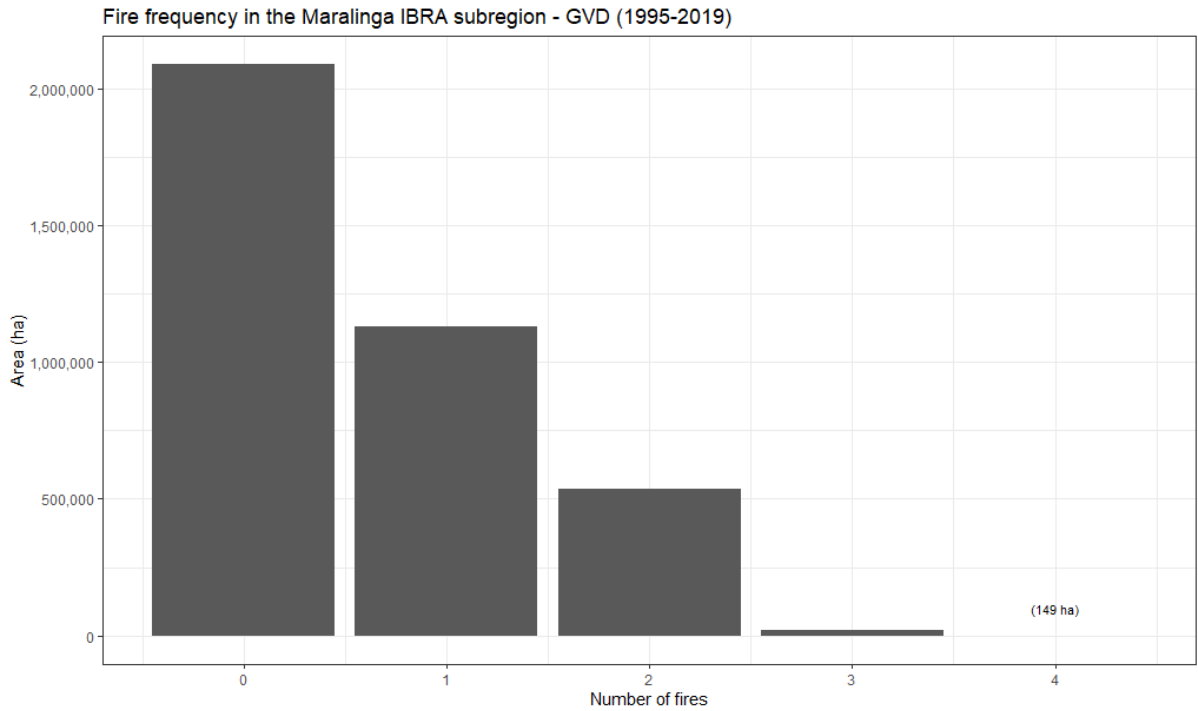


Figure 22: Fire frequency for the Maralinga IBRA region.

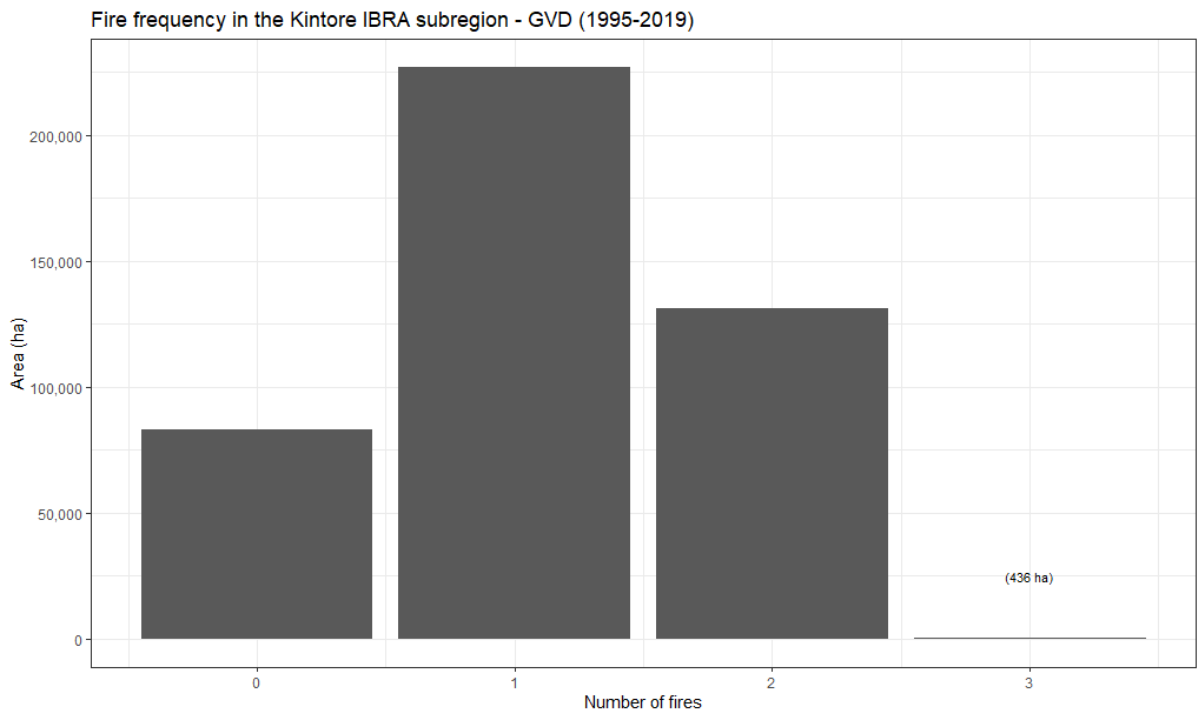


Figure 23: Fire frequency for the Kintore IBRA region.

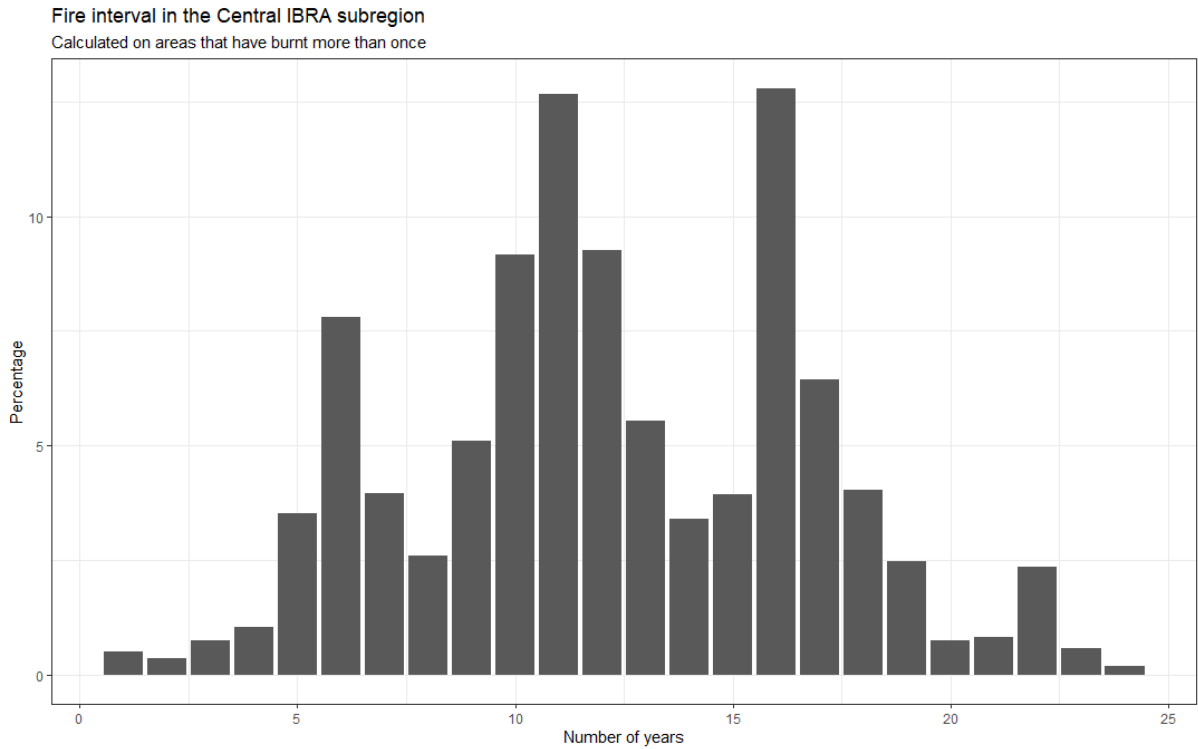


Figure 24: Fire interval for the Central IBRA region.

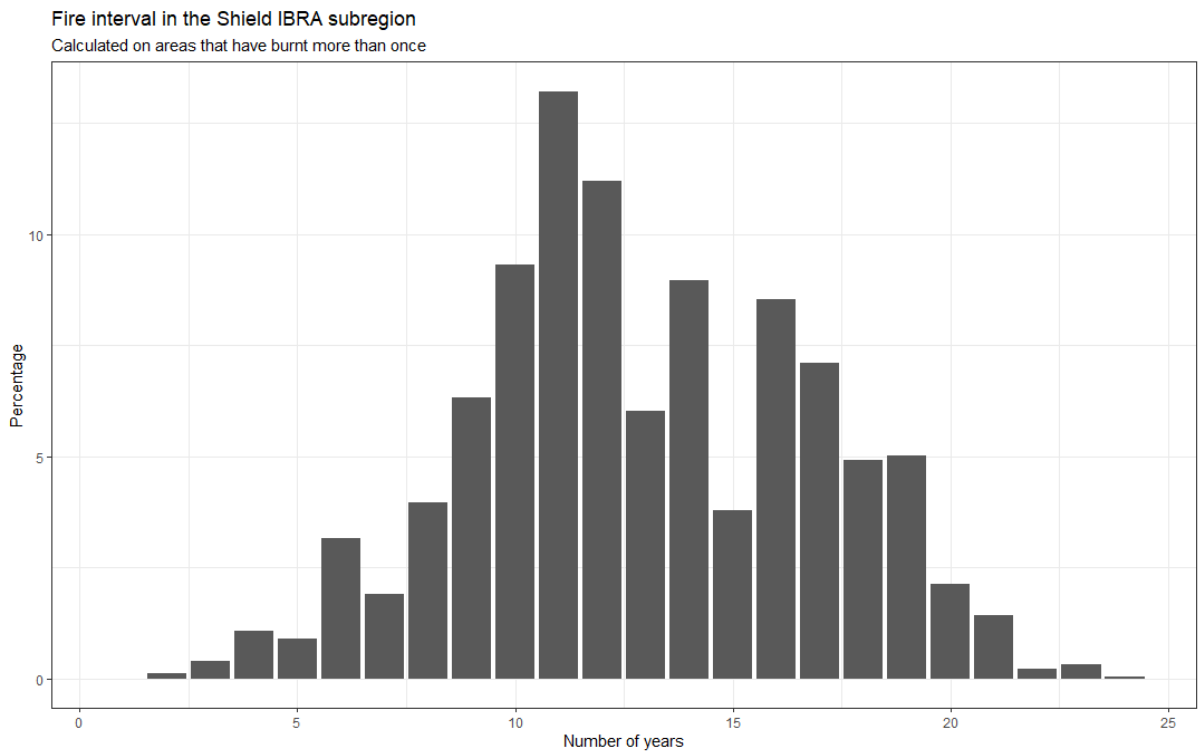


Figure 25: Fire interval for the Shield IBRA region.

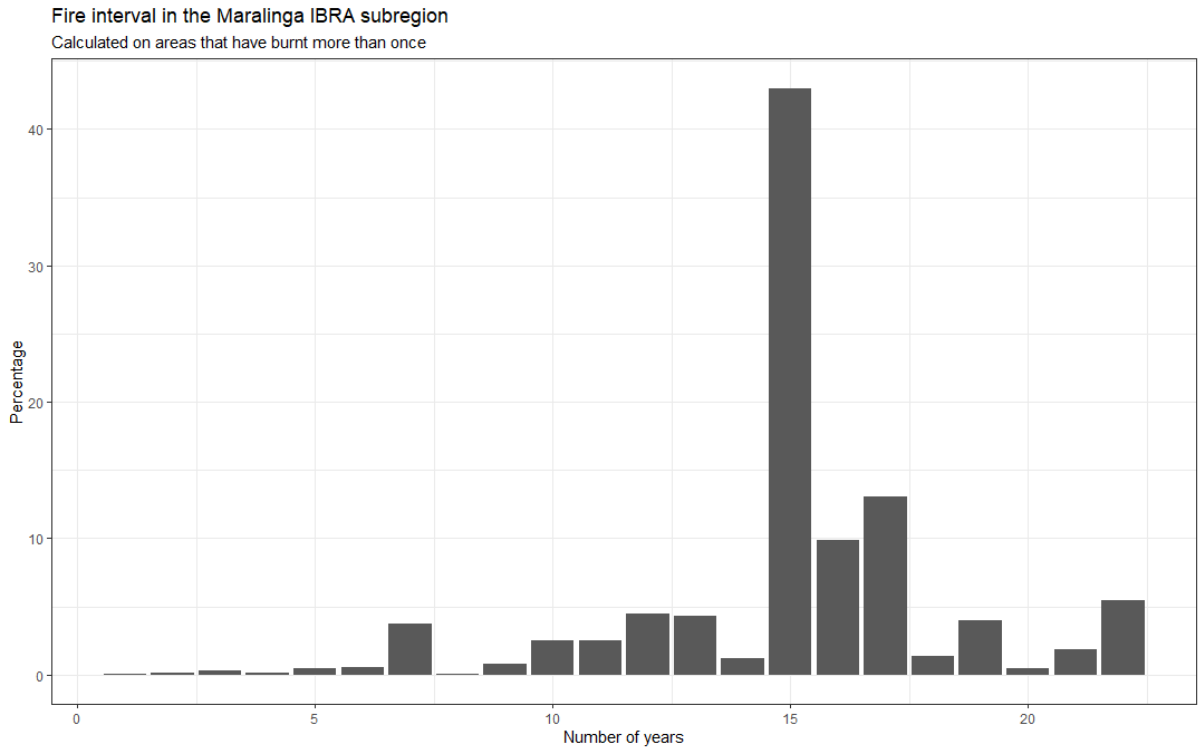


Figure 26: Fire interval for the Maralinga IBRA region.

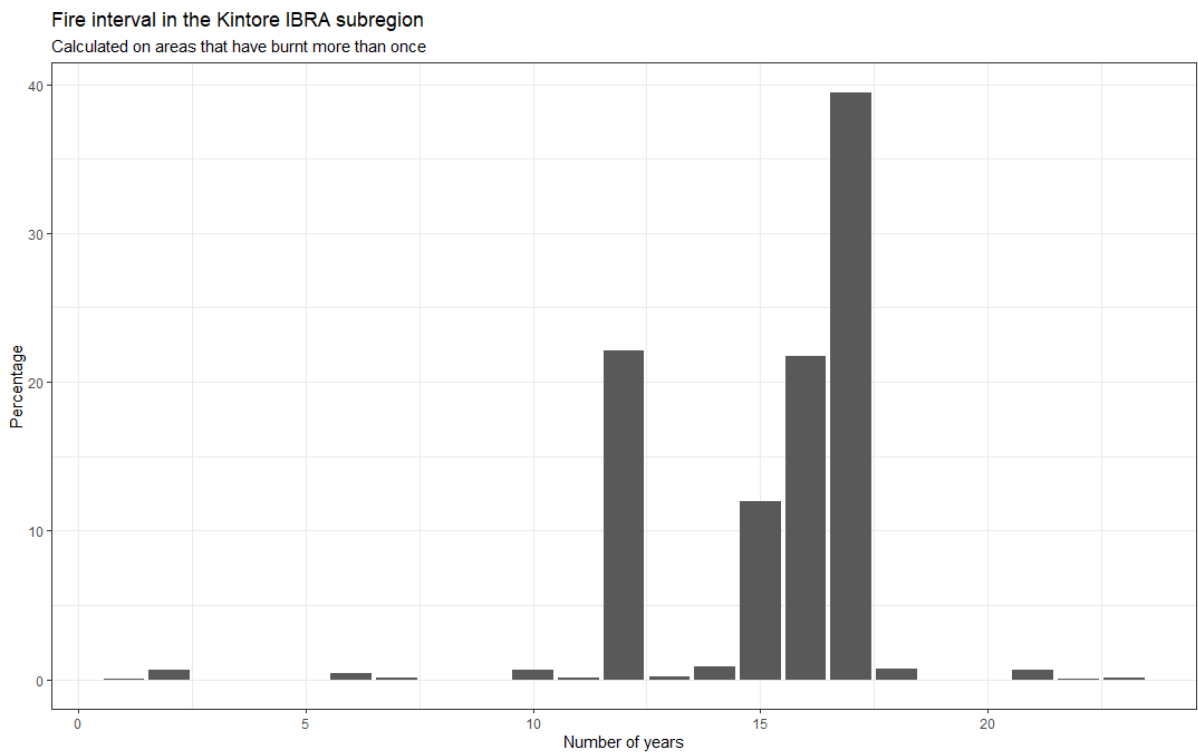


Figure 27: Fire interval for the Kintore IBRA region.

3.2 Plot scale fire and recovery

A description of the fire/recovery cycle can be analysed in detail at a plot scale. Time series graphs of vegetation cover estimates for areas that have burnt between zero and three times are shown in Figure 29 to Figure 32. The location of these plots is shown in Figure 28.

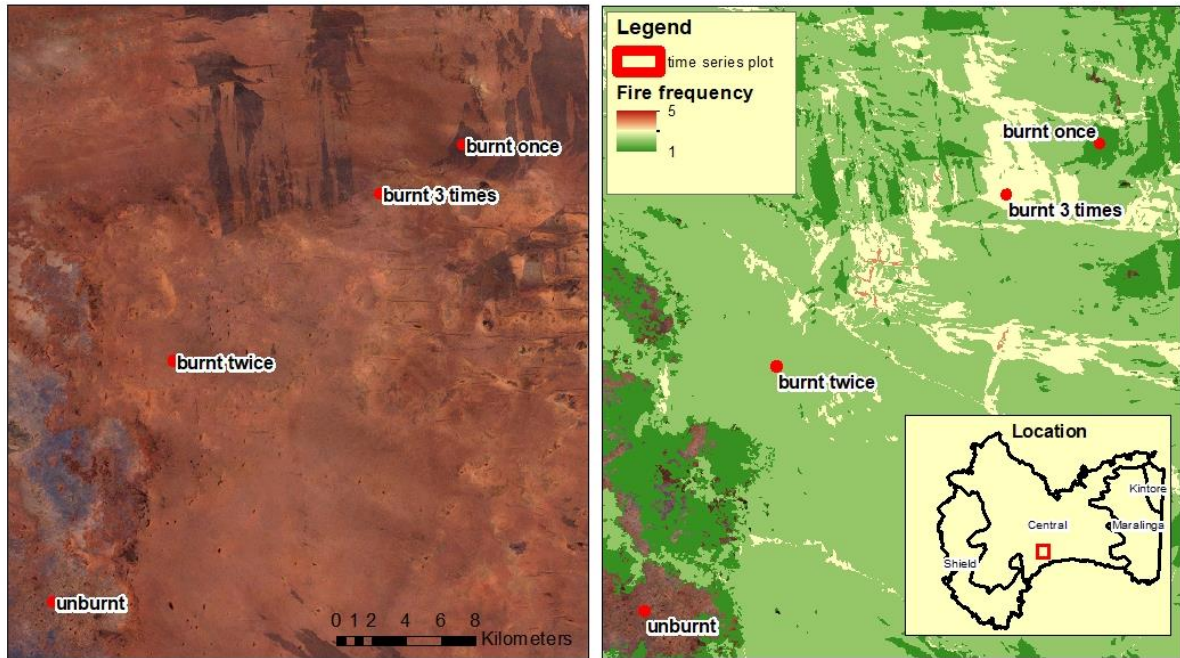


Figure 28: Location of time series plots.

Burn-recovery example: burnt 0 times

Vegetation cover algorithm created from aerial photography

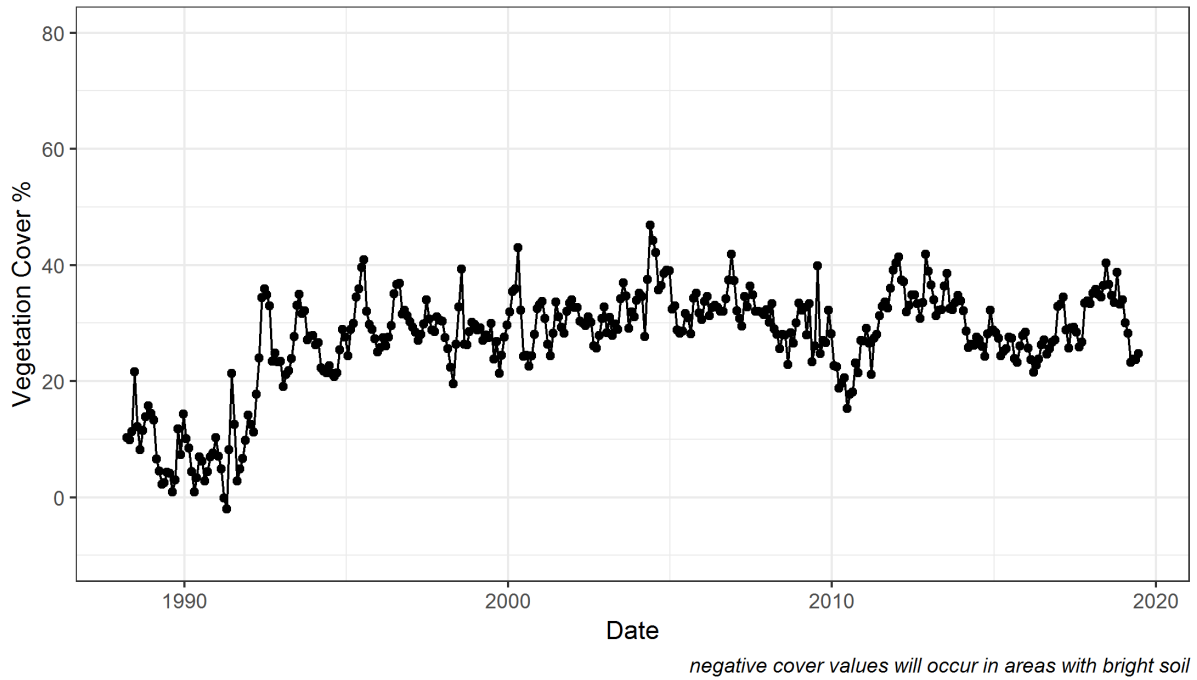


Figure 29: Time series graph of vegetation cover values for an area which did not burn in the 1995 to 2019 time period in Figure 28.

Burn-recovery example: burnt 1 times

Vegetation cover algorithm created from aerial photography

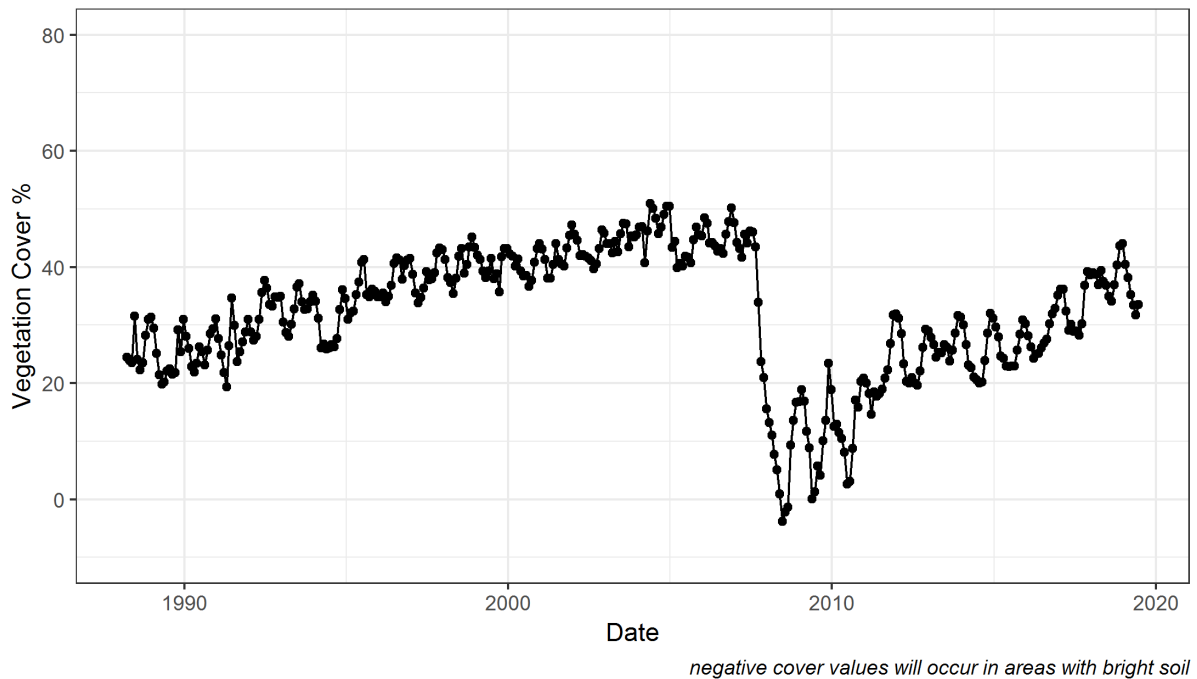


Figure 30: Time series graph of vegetation cover values for an area which burnt once in the 1995 to 2019 time period in Figure 28.

Burn-recovery example: burnt 2 times

Vegetation cover algorithm created from aerial photography

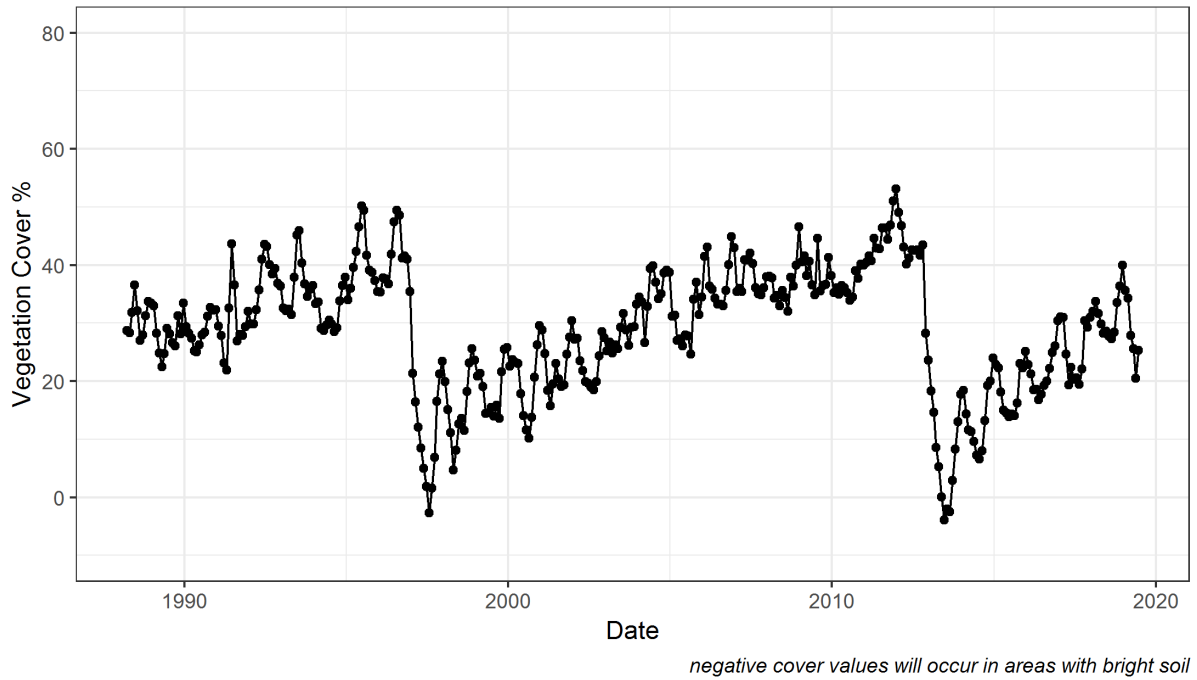


Figure 31: Time series graph of vegetation cover values for an area which burnt twice in the 1995 to 2019 time period in Figure 28.

Burn-recovery example: burnt 3 times

Vegetation cover algorithm created from aerial photography

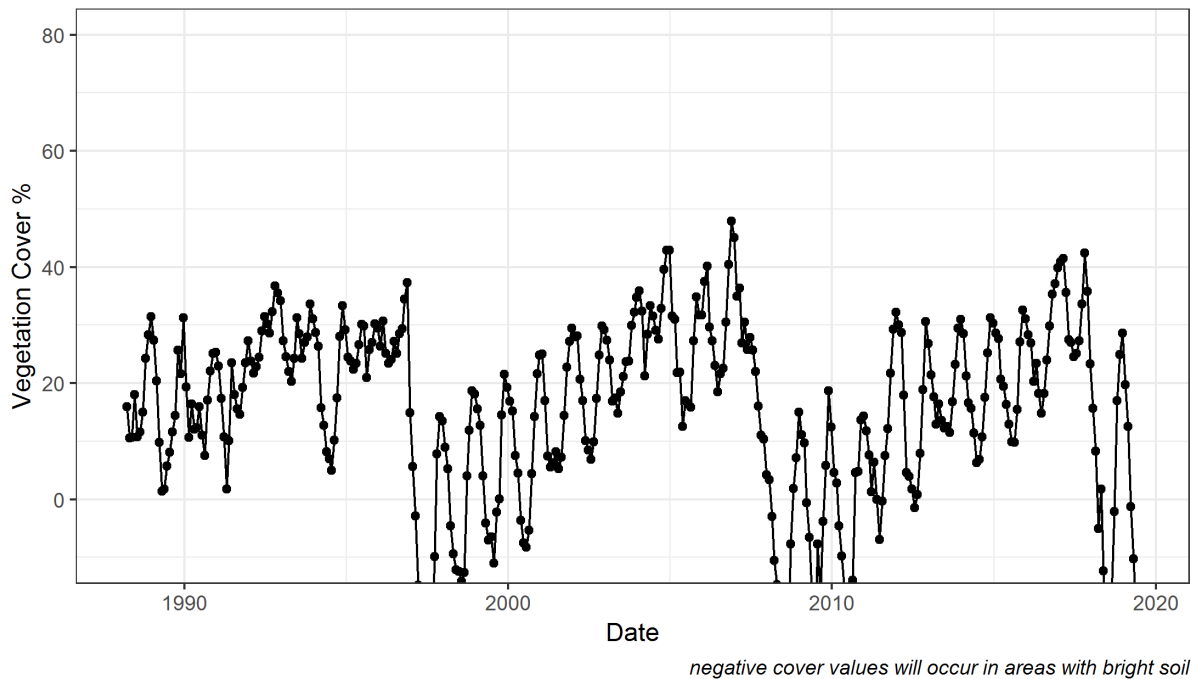


Figure 32: Time series graph of vegetation cover values for an area which burnt three times in the 1995 to 2018 time period.

3.3 DBCA Landsat-based and NAFI MODIS-based fire products: differences and causes

3.3.1 Summary

- The DBCA Landsat-based method has higher fire scar detection capacity and higher spatial resolution than the NAFI MODIS-based approach, resulting in improved fire-related landscape metrics.
- Burnt area measures derived from DBCA and NAFI fire products follow similar trends at a regional scale in the study area during the time period studied but differ significantly when looking at finer scales.
- Due to the resolution of the satellites used in the NAFI process there are significant omission errors, which in turn leads to significant errors in fuel age determination, both at large and small scales.
- NAFI and DBCA fire products should be used to inform different processes based on different spatial and temporal scale requirements. NAFI fire products are appropriate, among other, for assessing fire trends at a regional/sub-regional scale, while DBCA Landsat-based fire scars are also adequate to generate accurate landscape vegetation metrics, suitable to direct on ground operations and ecological studies

3.3.2 Study area

We conducted this study in the western sector of the Great Victoria Desert (Figure 33). This area includes Central and Shield IBRA subregions, as well as a fire management area and a reference area. Calculations in this report are presented in relation to the different geographical extents shown in Figure 33: Central, Shield, Reference and Management. The study period is 2000 to 2019, as NAFI data are available since 2000.

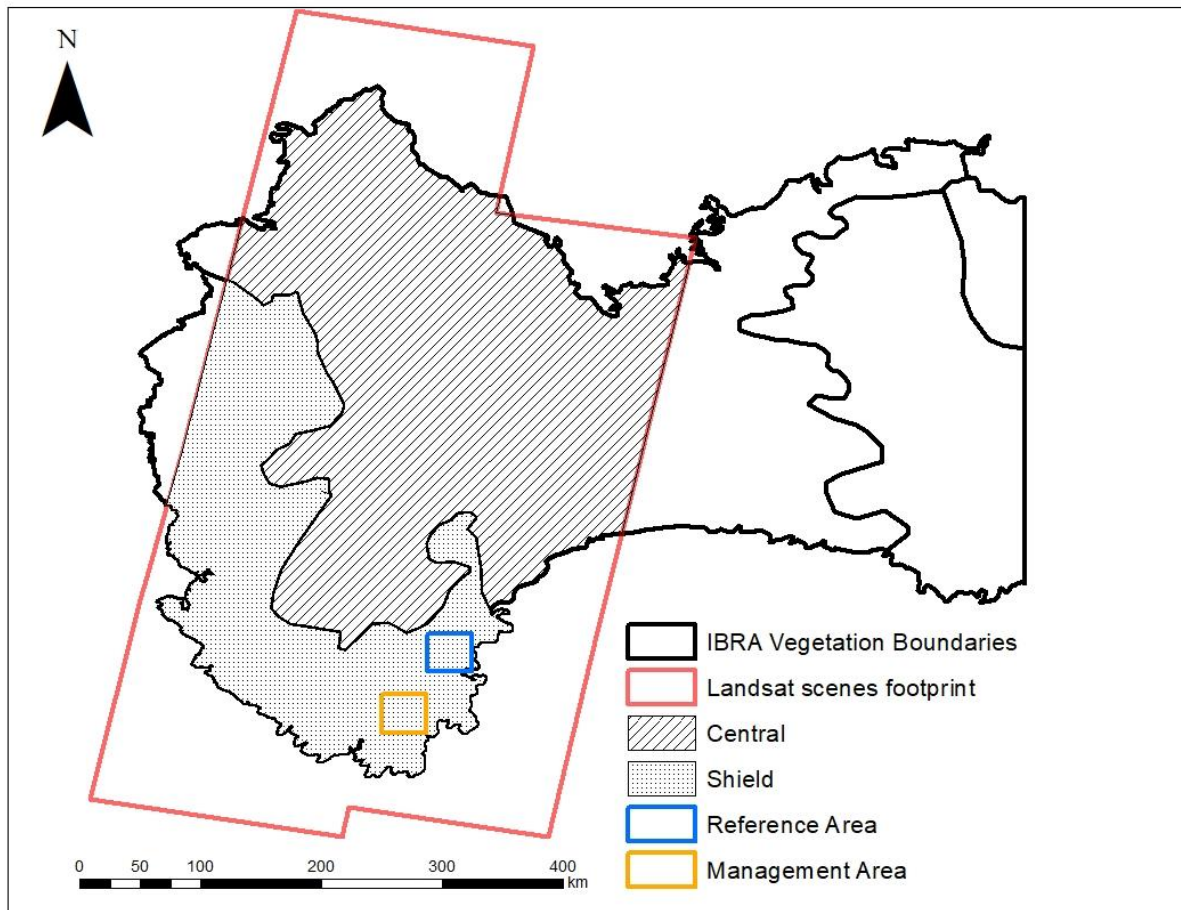


Figure 33. DBCA Landsat-based and NAFI MODIS-based fire product comparison: study area in the western sector of the Great Victoria Desert

3.3.3 Results

3.3.3.1 Burnt area comparisons

We analysed the proportion of the studied geographical extents that burnt at least once during the study period, using both DBCA and NAFI data. Results show that the DBCA Landsat-based method has higher fire detection capacity than the NAFI MODIS-based approach (Figure 34). We further computed all the overlapping and non-overlapping areas between both data sets and were able to calculate how much area was classified as burnt in one method and as unburnt in the other method. In this way, we were able to determine the extent of the two elements contributing to inaccuracies in the NAFI MODIS-based approach: a first component made of commission errors (areas that were classified as fire but that didn't actually burn) and a second component consisting of omission errors (areas that burnt but went undetected and appear as unburnt areas in the NAFI fire scar data set) (figure 34 red outline, and table 5).

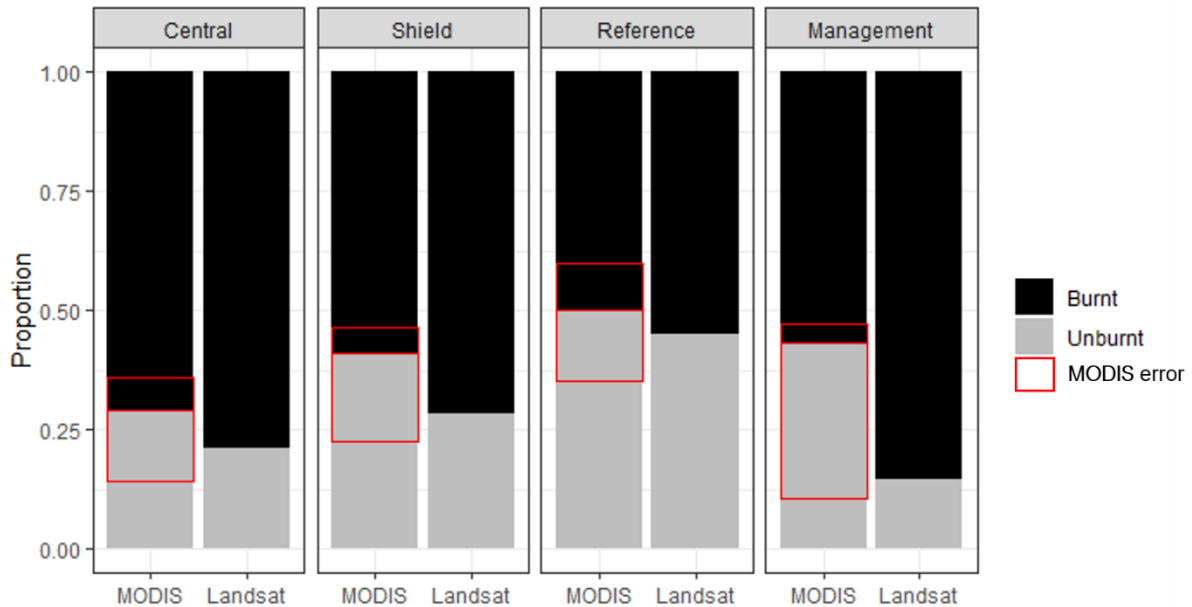


Figure 34. Proportion of different geographical extents that appear to have burnt at least once, from 2000 to 2019, derived from DBCA Landsat-based and NAFI MODIS-based fire products. Red outlines show commission errors (within burnt) and omission errors (within unburnt) of the NAFI MODIS-based method

Study Area	Type of error	Hectares	% of Study Area
Central	Commission	589,814	6.8
	Omission	1,281,965	14.7
Shield	Commission	243,574	5.7
	Omission	781,652	18.4
Reference	Commission	9,234	9.6
	Omission	14,322	14.9
Management	Commission	4,105	4.0
	Omission	33,273	32.8

Table 5. Number of hectares and proportion of each studied extent corresponding to the NAFI MODIS-based commission and omission errors.

When analysing data in a yearly basis, DBCA Landsat-derived burnt area calculations follow similar trends to NAFI MODIS-derived burnt areas. This is particularly true when looking at data across larger regional scales, such as the Central and Shield IBRA subregions (Figures 35 and 36), and to a lesser extent

when looking at smaller scales, such as the proposed fire management and reference areas in the south-western sector of the GVD (Figures 37 and 38). As an overall trend (with a few exceptions in certain years), DBCA Landsat-derived fire scars collectively add up to similar or larger total area burnt when compared to NAFI MODIS-derived fire scars for a particular year.

Here we must clarify a difference between both methods that, in some occasions, can end up in a fire being detected by both methods, but assigned to year n in the NAFI MODIS-based results, and to year $n+1$ in the DBCA Landsat-based results. NAFI generates fire scars in a monthly basis, taking advantage of MODIS's four passes-a-day over the same point. At DBCA, we haven't generated fire scars on a monthly basis, but on an annual basis.

To clarify the process of data analysis, in order to delineate fires that happened in 2019 (for example), we selected a cloud-free image from the end of 2019 and compare it with an image from the end of 2018. Ideally, we aim to obtain images from the last week of December, but that is not often possible due to the scheduled Landsat passes (every 16 days) and/or due to cloud cover. That is the reason why in many cases we have selected images from early December, November and in some cases October, so we can have a cloud-free scene. That means that a fire that happened in December 2018 might be included in the 2019 data, and a fire from December 2019 would be included in the 2020 data.

Consequently, assignment of a fire to a particular year using NAFI-generated data is more precise than with the DBCA method. While NAFI-based approach always covers a window from January to December of year n , DBCA Landsat-based approach covers variable windows from year to year (November of year n to November of year $n+1$ /November of year n to December of year $n+1$ /October of year n to December of year $n+1$, etc) depending on the timing of the used images (see Appendix). If a certain year saw large fires happening in late December, and we selected an image from November for that particular year, the differences in area burnt could be quite substantial with NAFI fire scars (although that fire will be included in the following year in the case of the DBCA fire scars). This explains why sometimes there seems to be a "lag" of 1 year between both methods. This difference is attenuated when we generate statistics such as "year since last burn" or fuel age maps, as differences in fuel age for a particular scar will be only 1 year.

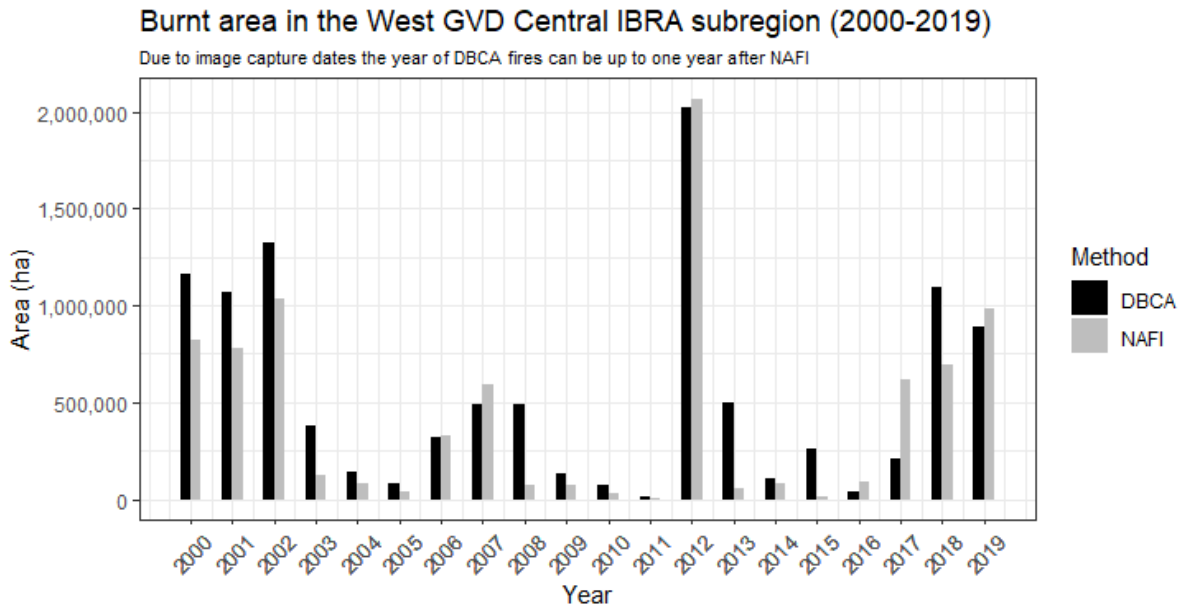


Figure 35. Annual burnt area in the West GVD Central IBRA subregion, from 2000 to 2019, derived from DBCA Landsat-based and NAFI MODIS-based fire products.

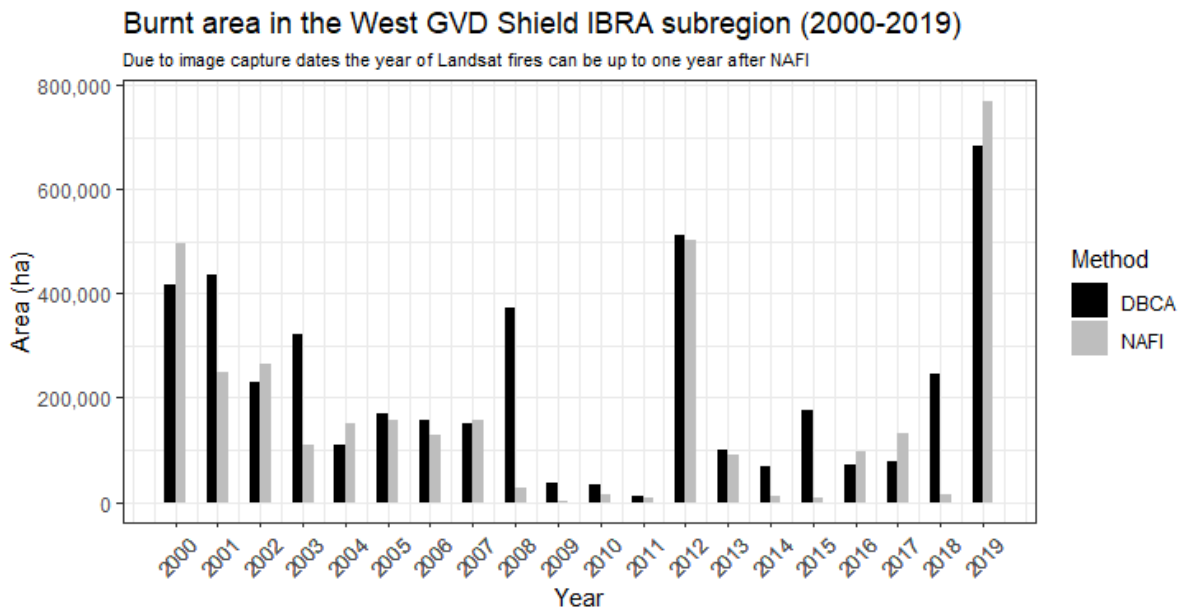


Figure 36. Annual burnt area in the West GVD Shield IBRA subregion, from 2000 to 2019, derived from DBCA Landsat-based and NAFI MODIS-based fire products.

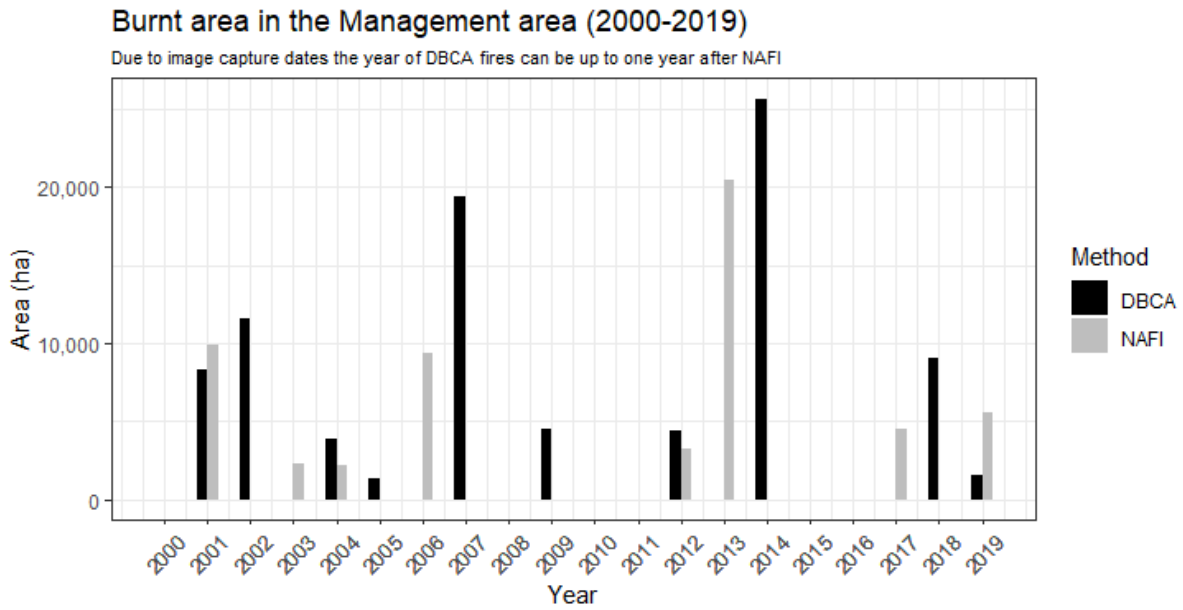


Figure 37. Annual burnt area in the proposed fire management area, from 2000 to 2019, derived from DBCA Landsat-based and NAFI MODIS-based fire products.

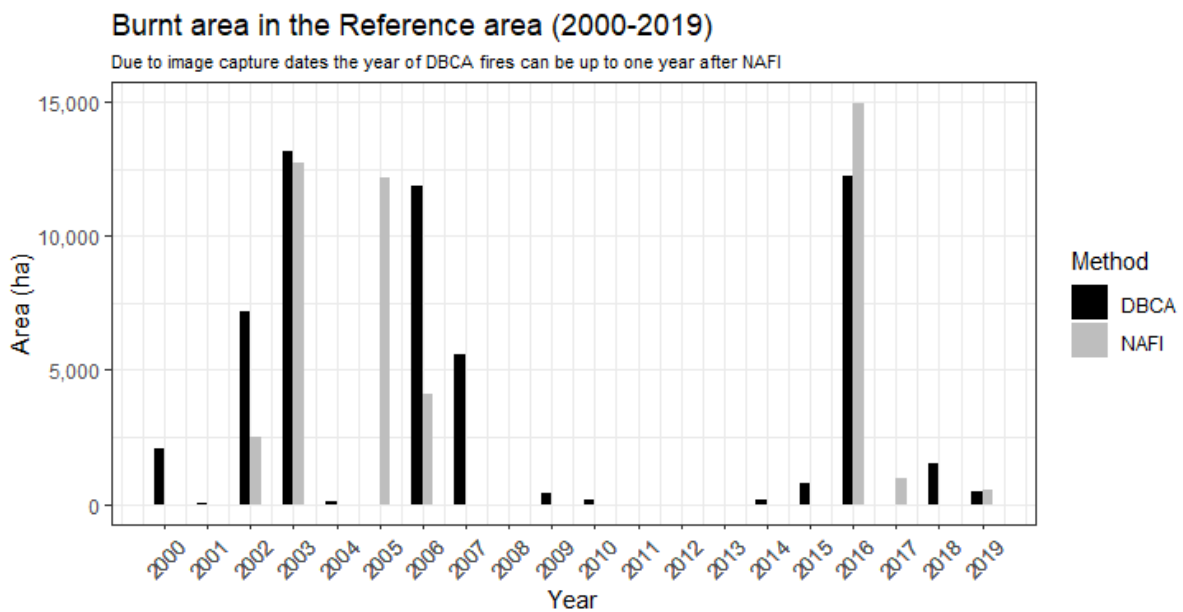


Figure 38. Annual burnt area in the proposed fire reference area, from 2000 to 2019, derived from DBCA Landsat-based and NAFI MODIS-based fire products.

3.3.3.2 Year since last burn comparisons

By overlaying the *year since last burn* results from both methods (which provide information about fuel age), we determined whether both methods provided the same *year since last burn* value, a difference of only 1 year, or a

difference of 2 or more years. Due to the 1-year lag possibility explained in section 3.3.3.1, we considered a difference of 2 or more years to be a disagreement between both method outputs. This is presented both as a proportion of the studied extents and in total area numbers (Figure 39 and Table 6).

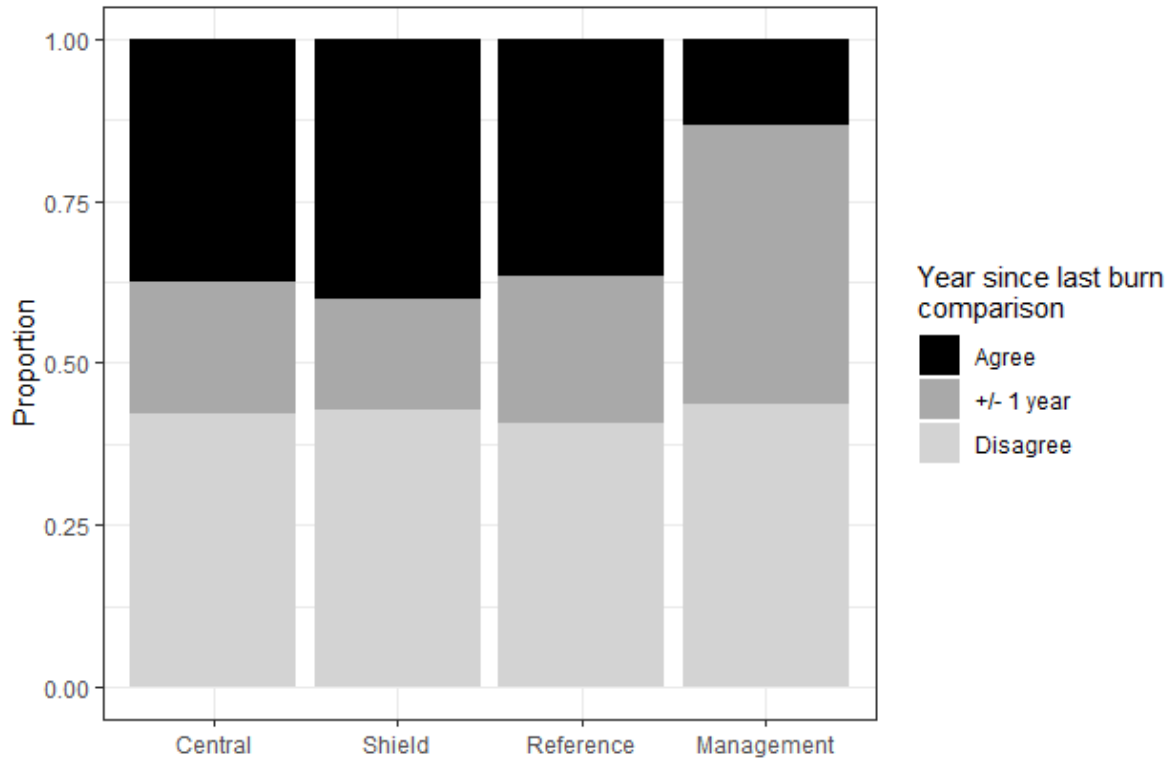


Figure 39. Proportion of the studied geographical extents in which there is an agreement, a difference of 1 year or a disagreement in year since last burn between DBCA Landsat-based and NAFI MODIS-based methods.

Study Area	YSLB	Hectares	% of Study Area
Central	Agree	2,796,535	37.5
	+/- 1 year	1,504,880	20.2
	Disagree	3,151,756	42.3
Shield	Agree	1,321,411	40.1
	+/- 1 year	569,631	17.3
	Disagree	1,405,653	42.6

Reference	Agree	22,790	36.7
	+/- 1 year	13,956	22.5
	Disagree	25,340	40.8
Management	Agree	11,985	13.2
	+/- 1 year	39,417	43.3
	Disagree	39,565	43.5

Table 6. Number of hectares and percentages of the studied geographical extents in which there is an agreement, a difference of 1 year or a disagreement in year since last burn (YSLB) between DBCA Landsat-based and NAFI MODIS-based methods.

When analysing data in a yearly basis, *year since last burn* statistics from DBCA and NAFI fire products also follow a similar overall trend over the two studied IBRA subregions (Figures 40 and 41). When looking at the scale of the proposed fire management and reference areas, trends are also alike, although more variable than across larger scales (Figures 42 and 43). In this latter case, when examining the spatial distribution of different fuel ages, it becomes clear that NAFI products could lead to an overestimation of fuel age (Figure 44). This relates to the NAFI MODIS-based detection inaccuracies shown in Figure 39. If a fire went undetected by NAFI, that part of the landscape might appear as having older vegetation than what it actually has. For example, if it burnt 10 years ago and then again 5 years ago, but this second burn went undetected, it will appear as being 10 years old, when it is actually 5 years old. In Figure 51 we can see that many areas that appear unburnt in NAFI (in white), and that we would therefore assume have at least 19 year old fuel, have actually younger vegetation because they did burn at some point in the last 19 years (as shown in the Landsat-based map).

To further develop this point, Figure 45 shows a simulation using 5 randomly located points within the proposed fire management area. In it, we assume that in 2000 all of those 5 points were in areas that had just been burnt, which means their fuel age was 0. Using the DBCA Landsat-derived and the NAFI MODIS-derived fire scars, we monitored the change in fuel age in those 5 check points from 2000 to 2019. At the end of the study period, we can see that 3 of the points are within 1 year of fuel age of each other (points 1, 2 and 4), reflecting a fire passed through this point. However, points 3 and 5 fall within areas where the NAFI MODIS-based method missed recording a fire during the study period, which translates to an over-estimation of fuel age by the NAFI MODIS-based method of 7 and 9 years, respectively.

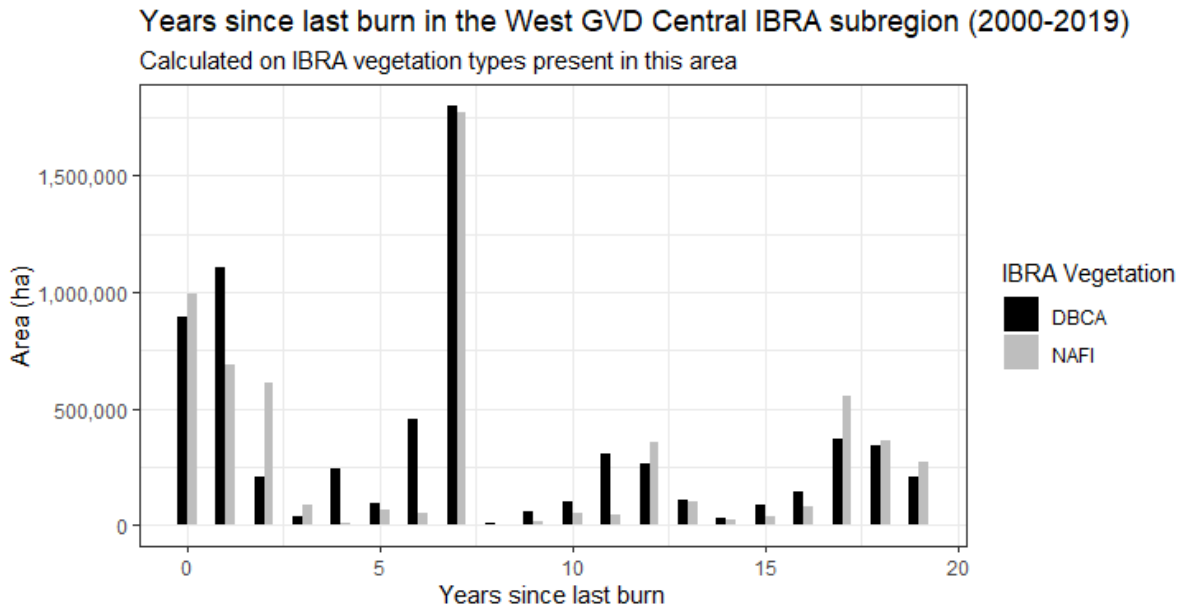


Figure 40. Fuel age area distribution calculated as years since last burn in the West GVD Central IBRA bioregion, from 2000 to 2019, derived from DBCA Landsat-based and NAFI MODIS-based fire products.

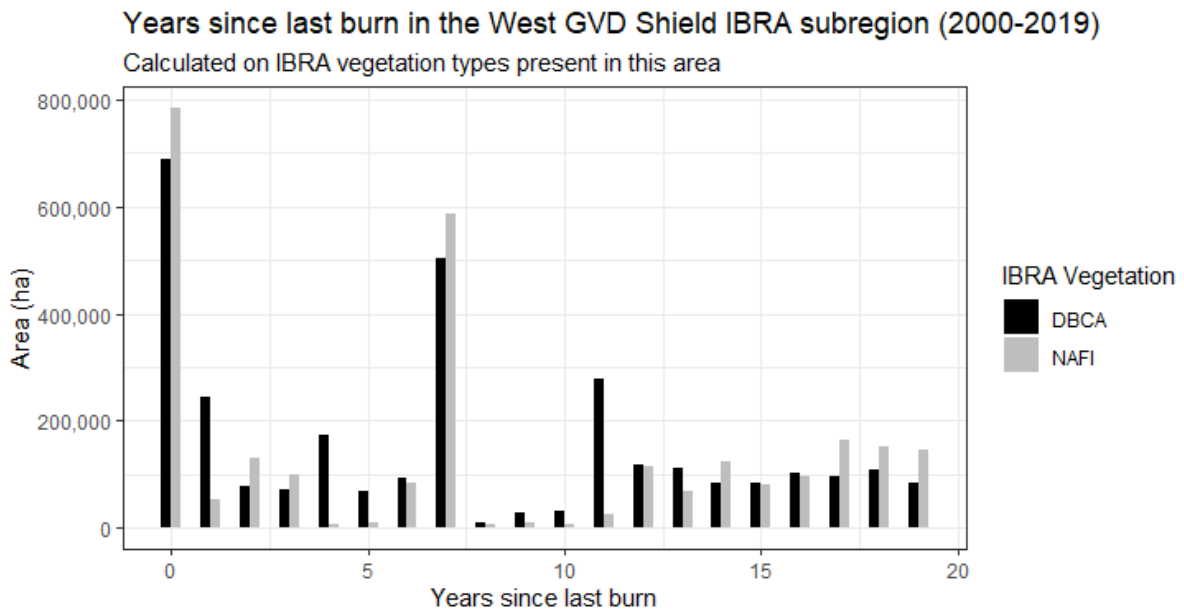


Figure 41. Fuel age area distribution calculated as years since last burn in the West GVD Shield IBRA bioregion, from 2000 to 2019, DBCA Landsat-based and NAFI MODIS-based fire products.

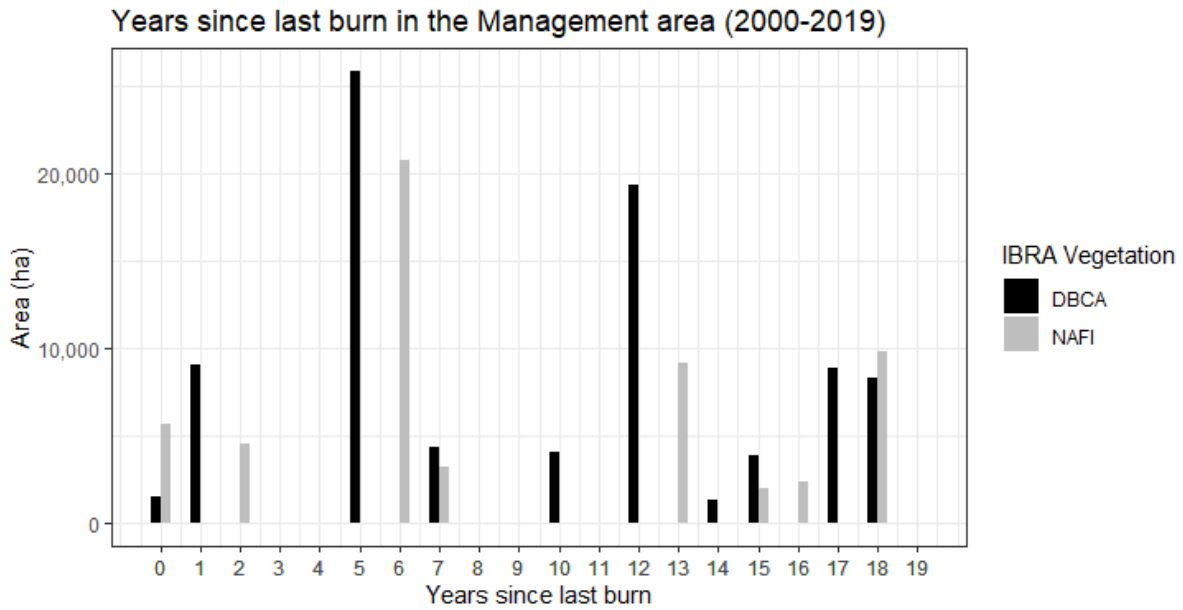


Figure 42. Fuel age area distribution calculated as years since last burn in the proposed fire management area, from 2000 to 2019, DBCA Landsat-based and NAFI MODIS-based fire products.

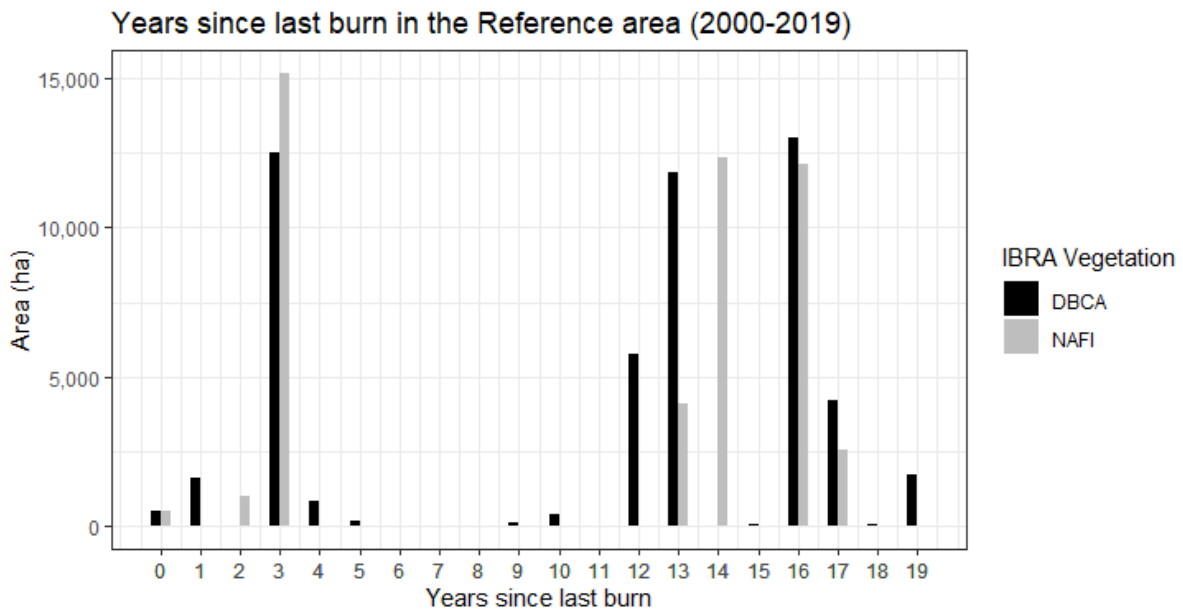


Figure 43. Fuel age area distribution calculated as years since last burn in the proposed fire reference area, from 2000 to 2019, DBCA Landsat-based and NAFI MODIS-based fire products.

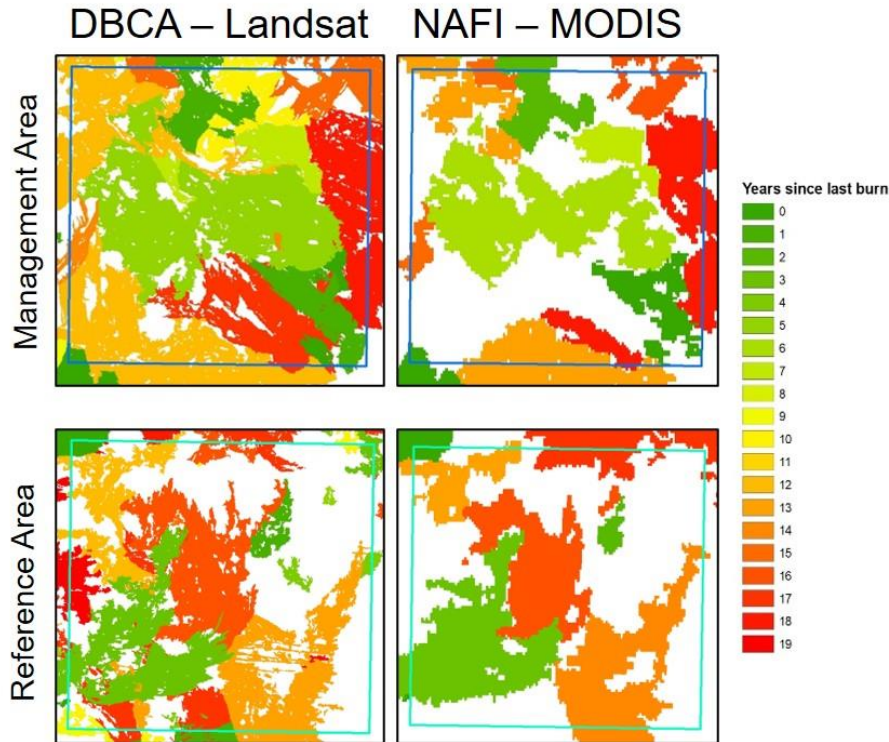


Figure 44. Fuel age spatial distribution calculated as years since last burn in the proposed fire management and reference areas, from 2000 to 2019, DBCA Landsat-based and NAFI MODIS-based fire products.

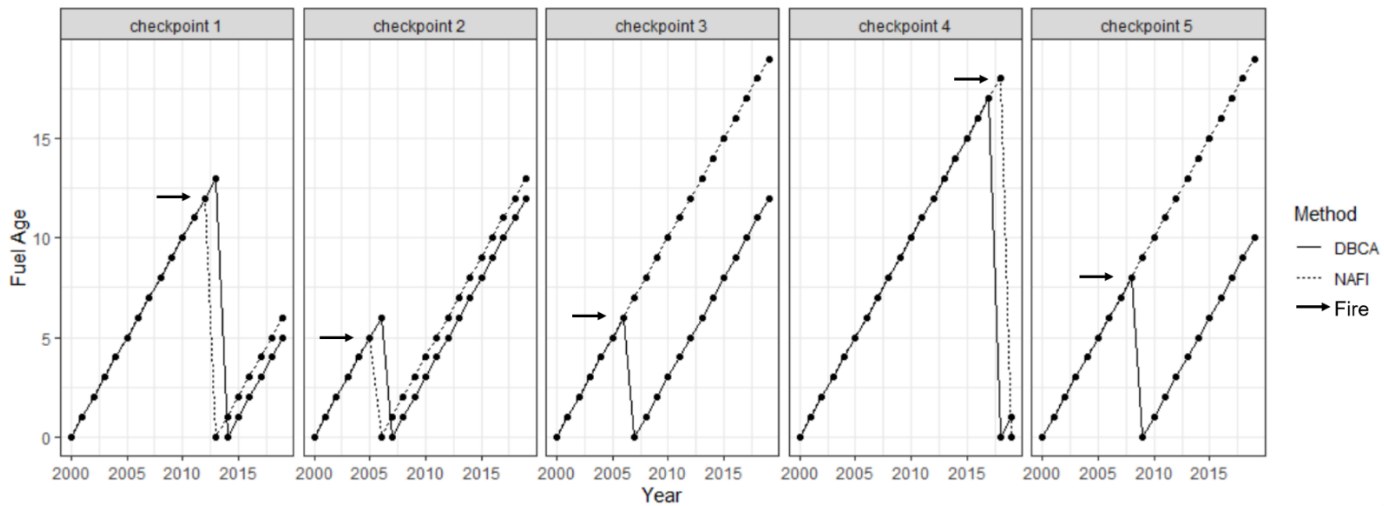


Figure 45. Fuel age simulation on 5 randomly located points within the fire management area, using DBCA Landsat-based and NAFI MODIS-based fire products.

3.3.3.3 *Fire scar comparisons*

A detailed analysis of all DBCA and NAFI overlapping fire scars across the breadth of the subregions has not been performed. However, a few DBCA generated fire scars have been compared with NAFI generated fire scars in the same area on the same year to highlight some inconsistencies in the different spatial analyses (Figure 46). Compared scars have been chosen either for their relative difference and/or for characteristics that allow for visual clarity. Figure 46.A shows a large 2008 fire scar that only appears to have been partially detected through the NAFI workflow (and is not present in the previous-year NAFI scar either). This scar contributed to significant differences in burnt area calculations between DBCA and NAFI within the Shield IBRA subregion in 2008. Figure 46.B shows how NAFI and DBCA methods provided different results for this particular fire of 2017, with the NAFI MODIS-based method not picking up the eastern part of the fire (also not present in the previous year NAFI fire scar). Figure 46.C and 46.D show clear differences in 2017 and 2018 fire scars respectively, particularly in delineating finer structure and patchiness of smaller sized fires. Finally, figures 46.E and 46.F show two areas where DBCA and NAFI did a very similar job at delineating actual fires in 2018, but the NAFI workflow missed two water bodies that were classified as burned areas.

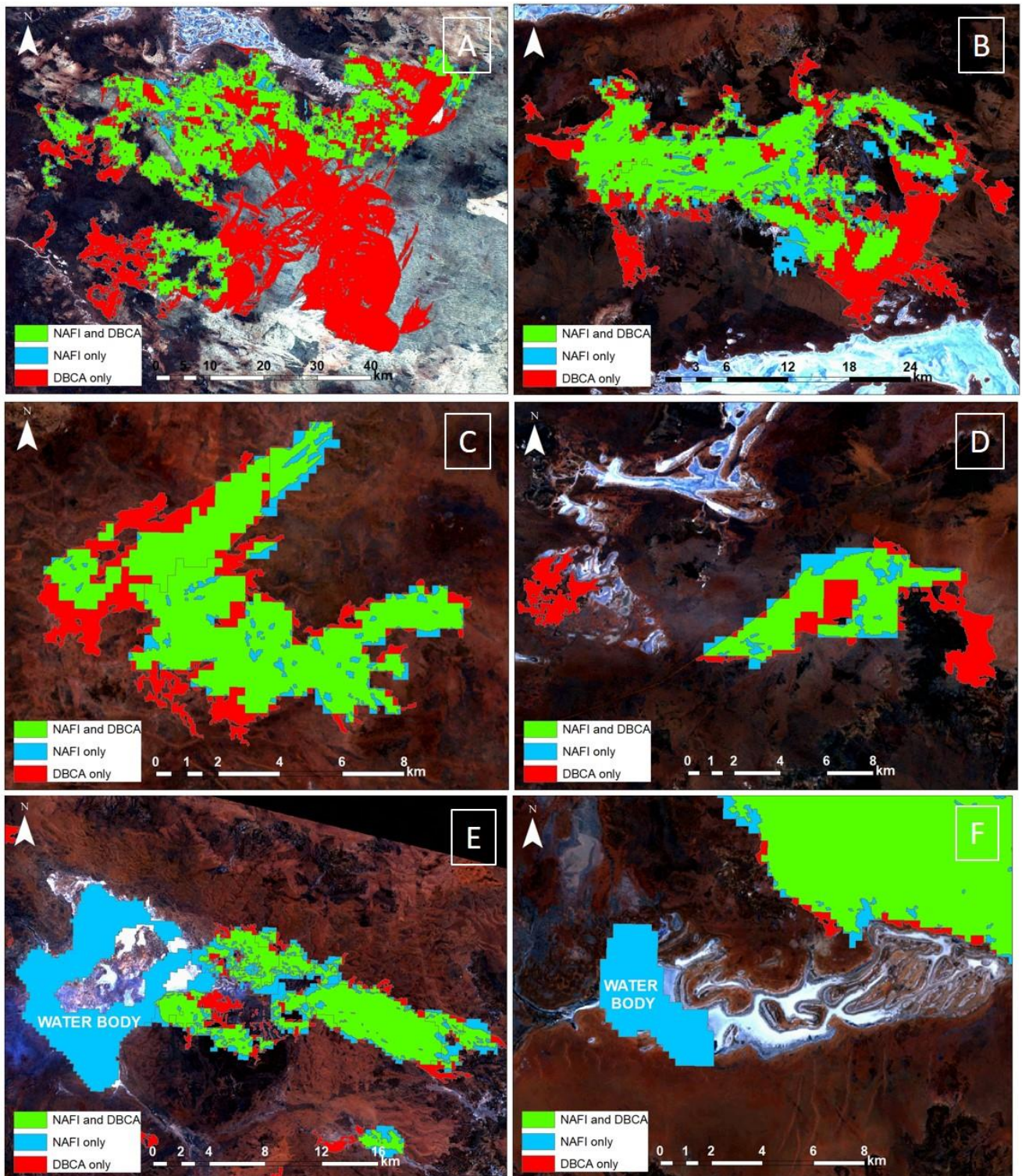


Figure 46. Fire scar overlap and intersections between DBCA Landsat-based and NAFI MODIS-based fire products across different areas of the West GVD in 2008 (A), 2017 (B,C) and 2018 (D,E and F).

3.3.4 Discussion

Differences between DBCA Landsat-based and NAFI MODIS-based fire products within our study area can be explained, to a certain extent, through technical and methodological arguments.

In order to delineate fire scars NAFI uses differences in the MODIS satellite 250 m near-infrared band (NIR, 841 – 876 nm), through an object-oriented segmentation process. DBCA also uses an object-oriented segmentation process, but based on 30 m resolution Landsat images processed into two different burn indices, a Landsat near infra red band difference (NIR, 760 – 900 nm, varying slightly across different Landsat missions) and a Normalised Burn Ratio index, (near infrared – short-wave infrared) / (near infrared + short-wave infrared) (short-wave infrared band covering the wavelengths 2100 – 2300 nm, varying slightly across different Landsat missions).

For these reasons, we assume that DBCA Landsat-based fire products have higher spatial accuracy (250 m MODIS vs 30 m Landsat pixel size) and higher detection capacity (1 index MODIS vs 2 indices Landsat). Ground truthing to determine the accuracy of DBCA Landsat-derived data within the GVD would be a valuable further study.

Higher detection capacity explains why the overall trend is that DBCA Landsat-based fire scars account for larger total burn areas when compared to NAFI MODIS-based fire scars across both larger and smaller spatial scales (Figures 34 to 39). In this regard, fire scar detection challenges in arid landscapes, such as the GVD, are acknowledged by NAFI in their *Extending NAFI Fire History Mapping* report (Jacklyn, 2017) to the GVD Biodiversity Trust: "... when sparse vegetation on highly reflective sandy landscapes are burnt – the fire initially produces a darkening and reduced reflectance due to the burnt vegetation, but then the vegetation can be blown away and the now exposed bare sand produces an increase in reflectance". Pointing in a similar direction, *The NAFI booklet* (Jacklyn, 2016) states that, while overall accuracy of NAFI fire scars lays between 85 and 90% (assessed through aerial survey), accuracy is lower in what they refer to as "more developed landscapes" in the southern part of its working extent.

All these factors lead to higher precision landscape metrics, such as fuel age, being provided by the DBCA Landsat-based method (Figures 45 and 46).

3.3.5 Conclusions

NAFI and DBCA-derived fire products should be used to inform different processes based on different spatial and temporal scale requirements. NAFI products are a valid tool to outline general fire trends at regional and sub-regional scales.

Additionally, its high temporal and low spatial resolutions allow the monitoring of active fires (and subsequent emergency decision support) as well as entire states to be mapped by a single human mapper once or twice a week, respectively. However, undetected fires by the NAFI MODIS-based method might lead to errors in fire-related landscape metrics, such as fuel age, both at larger and smaller spatial

scales. In contrast, fire scars provided by DBCA require a higher workload to process the data analyses but provide higher spatial and detection accuracies within the specific landscape conditions of the GVD. This results in improved fine structure, vegetation patchiness and fuel age determination, which could be essential in the context of ecological studies and ground operations within the GVD.

References

Jacklyn, P. (2017): *Extending NAFI Fire History Mapping*. Darwin Centre for Bushfire Research, Charles Darwin University, Darwin.

Jacklyn, P (2016): *The NAFI booklet*. Darwin Centre for Bushfire Research, Charles Darwin University, Darwin.

Kettig, R. L., & Landgrebe, D. A. (1976). *Classification of multispectral image data by extraction and classification of homogeneous objects*. IEEE Transactions on geoscience Electronics, 14(1), 19-26.

Key, C. H., & Benson, N. C. (1999). *The Normalized Burn Ratio (NBR): A Landsat TM radiometric measure of burn severity*. United States Geological Survey, Northern Rocky Mountain Science Center. (Bozeman, MT).

Thackway, R and Cresswell, I.D. (1995) *An interim biogeographic regionalisation for Australia: a framework for setting priorities in the National Reserves System Cooperative Program, Version 4.0*. Australian Nature Conservation Agency, Canberra.

Zdunic, K. and Huntley, B. (2015). *Meelup Regional Park Vegetation Monitoring using Multi-spectral Imagery*. Department of Biodiversity, Conservation and Attractions, Perth.

Appendix 1

Image dates for 107/80

year	date	satellite
1994	16/11/1994	Landsat 5
1995	5/12/1995	Landsat 5
1996	7/12/1996	Landsat 5
1997	26/12/1997	Landsat 5
1998	11/11/1998	Landsat 5
1999	26/08/1999	Landsat 5
2000	26/12/2000	Landsat 7
2001	11/11/2001	Landsat 7
2002	14/11/2002	Landsat 7
2003	11/12/2003	Landsat 5
2004	11/11/2004	Landsat 5
2005	29/10/2005	Landsat 5
2006	29/08/2006	Landsat 5
2007	3/10/2007	Landsat 5
2008	5/10/2008	Landsat 5
2009	25/11/2009	Landsat 5
2010	28/11/2010	Landsat 5
2011	23/11/2011	Landsat 7
2012	8/10/2012	Landsat 7
2013	1/09/2013	Landsat 8
2014	22/10/2014	Landsat 8
2015	28/12/2015	Landsat 8
2016	30/12/2016	Landsat 8
2017	30/10/2017	Landsat 8
2018	5/01/2019	Landsat 8
2019	7/12/2019	Landsat 8

Image dates for 107/81

1994	16/11/1994	Landsat 5
1995	16/09/1995	Landsat 5
1996	7/12/1996	Landsat 5
1997	26/12/1997	Landsat 5
1998	11/11/1998	Landsat 5
1999	26/08/1999	Landsat 5
2000	26/12/2000	Landsat 7
2001	11/11/2001	Landsat 7
2002	29/10/2002	Landsat 7
2003	11/12/2003	Landsat 5
2004	11/11/2004	Landsat 5
2005	29/10/2005	Landsat 5
2006	29/08/2006	Landsat 5
2007	17/09/2007	Landsat 5
2008	19/09/2008	Landsat 5
2009	25/11/2009	Landsat 5
2010	28/11/2010	Landsat 5
2011	23/11/2011	Landsat 7
2012	9/11/2012	Landsat 7
2013	11/10/2013	Landsat 7
2013	12/11/2013	Landsat 7
2014	22/10/2014	Landsat 8
2015	28/12/2015	Landsat 8
2016	30/12/2016	Landsat 8
2017	30/10/2017	Landsat 8
2018	5/01/2019	Landsat 8
2019	21//11/2019	Landsat 8

Image dates for 108/80

1994	7/11/1994	Landsat 5
1995	26/11/1995	Landsat 5
1996	28/11/1996	Landsat 5
1997	1/12/1997	Landsat 5
1998	20/12/1998	Landsat 5
1999	18/09/1999	Landsat 5
2000	14/10/2000	Landsat 7
2001	14/08/2001	Landsat 7
2002	4/10/2002	Landsat 7
2003	18/12/2003	Landsat 5
2004	4/12/2004	Landsat 5
2005	21/11/2005	Landsat 5
2006	7/10/2006	Landsat 5
2007	24/09/2007	Landsat 5
2008	26/09/2008	Landsat 5
2009	15/10/2009	Landsat 5
2010	19/11/2010	Landsat 5
2011	30/11/2011	Landsat 7
2012	2/12/2012	Landsat 7
2013	11/11/2013	Landsat 8
2014	27/09/2014	Landsat 8
2015	16/10/2015	Landsat 8
2016	19/11/2016	Landsat 8
2017	22/11/2017	Landsat 8
2018	25/11/2018	Landsat 8
2019	28/11/2019	Landsat 8

Image dates for 108/81

1994	7/11/1994	Landsat 5
1995	26/11/1995	Landsat 5
1996	28/11/1996	Landsat 5
1997	1/12/1997	Landsat 5
1998	4/12/1998	Landsat 5
1999	20/10/1999	Landsat 5
2000	14/10/2000	Landsat 7
2001	20/12/2001	Landsat 7
2002	4/10/2002	Landsat 7
2003	18/12/2003	Landsat 5
2004	4/12/2004	Landsat 5
2005	21/11/2005	Landsat 5
2006	21/09/2006	Landsat 5
2007	24/09/2007	Landsat 5
2008	10/09/2008	Landsat 5
2009	18/12/2009	Landsat 5
2010	19/11/2010	Landsat 5
2011	14/11/2011	Landsat 7
2012	2/12/2012	Landsat 7
2013	11/11/2013	Landsat 8
2014	27/09/2014	Landsat 8
2015	30/09/2015	Landsat 8
2016	19/11/2016	Landsat 8
2017	22/11/2017	Landsat 8
2018	25/11/2018	Landsat 8
2019	28/11/2019	Landsat 8

Image dates for 108/78

1994	22/10/1994	Landsat 5
1995	26/11/1995	Landsat 5
1996	27/10/1996	Landsat 5
1997	1/12/1997	Landsat 5
1998	17/10/1998	Landsat 5
1999	18/09/1999	Landsat 5
2000	14/10/2000	Landsat 7
2001	20/12/2001	Landsat 7
2002	20/10/2002	Landsat 7
2003	2/12/2003	Landsat 5
2004	4/12/2004	Landsat 5
2005	5/11/2005	Landsat 5
2006	26/12/2006	Landsat 5
2007	24/09/2007	Landsat 5
2008	13/11/2008	Landsat 5
2009	29/09/2009	Landsat 5
2010	3/11/2010	Landsat 5
2011	19/09/2011	Landsat 5
2012	15/10/2012	Landsat 5
2013	10/10/2013	Landsat 8
2014	30/11/2014	Landsat 8
2015	30/09/2015	Landsat 8
2016	19/11/2016	Landsat 8
2017	8/12/2017	Landsat 8
2018	25/11/2018	Landsat 8
2019	28/11/2019	Landsat 8

Image dates for 108/79

1994	7/11/1994	Landsat 5
1995	26/11/1995	Landsat 5
1996	14/12/1996	Landsat 5
1997	1/12/1997	Landsat 5
1998	17/10/1998	Landsat 5
1999	18/09/1999	Landsat 5
2000	14/10/2000	Landsat 7
2001	20/12/2001	Landsat 7
2002	5/11/2002	Landsat 7
2003	2/12/2003	Landsat 5
2004	4/12/2004	Landsat 5
2005	5/11/2005	Landsat 5
2006	10/12/2006	Landsat 5
2007	24/09/2007	Landsat 5
2008	13/11/2008	Landsat 5
2009	2/12/2009	Landsat 5
2010	19/11/2010	Landsat 5
2011	19/09/2011	Landsat 5
2012	18/12/2012	Landsat 5
2013	10/10/2013	Landsat 8
2014	30/11/2014	Landsat 8
2015	30/09/2015	Landsat 8
2016	19/11/2016	Landsat 8
2017	22/11/2017	Landsat 8
2018	25/11/2018	Landsat 8
2019	28/11/2019	Landsat 8

Image dates for 107/79

1994	16/11/1994	Landsat 5
1995	5/12/1995	Landsat 5
1996	7/12/1996	Landsat 5
1997	10/12/1997	Landsat 5
1998	27/11/1998	Landsat 5
1999	26/08/1999	Landsat 5
2000	26/12/2000	Landsat 7
2001	29/12/2001	Landsat 7
2002	14/11/2002	Landsat 7
2003	8/10/2003	Landsat 5
2004	11/11/2004	Landsat 5
2005	29/10/2005	Landsat 5
2006	1/11/2006	Landsat 5
2007	17/09/2007	Landsat 5
2008	5/10/2008	Landsat 5
2009	25/11/2009	Landsat 5
2010	14/12/2010	Landsat 5
2011	28/09/2011	Landsat 5
2012	9/11/2012	Landsat 5
2013	1/09/2013	Landsat 8
2014	9/12/2014	Landsat 8
2015	23/09/2015	Landsat 8
2016	12/11/2016	Landsat 8
2017	30/10/2017	Landsat 8
2018	17/10/2018	Landsat 8
2019	21/11/2019	Landsat 8

Image dates for 106/80

1994	25/11/1994	Landsat 5
1995	28/11/1995	Landsat 5
1996	14/11/1996	Landsat 5
1997	1/11/1997	Landsat 5
1998	22/12/1998	Landsat 5
1999	14/10/1999	Landsat 7
2000	14/09/2000	Landsat 7
2001	17/09/2001	Landsat 7
2002	20/09/2002	Landsat 7
2003	2/11/2003	Landsat 5
2004	19/10/2004	Landsat 5
2005	15/05/2005	Landsat 5
2006	2/05/2006	Landsat 5
2007	5/05/2007	Landsat 5
2008	12/09/2008	Landsat 5
2009	30/08/2009	Landsat 5
2010	13/05/2010	Landsat 5
2011	21/09/2011	Landsat 5
2012	1/10/2012	Landsat 5
2013	26/09/2013	Landsat 8
2014	28/08/2014	Landsat 8
2015	16/09/2015	Landsat 8
2016	18/09/2016	Landsat 8
2017	26/12/2017	Landsat 8
2018	13/12/2018	Landsat 8
2019	14/11/2019	Landsat 8

Image dates for 106/79

1994	25/11/1994	Landsat 5
1995	28/11/1995	Landsat 5
1996	14/11/1996	Landsat 5
1997	19/12/1997	Landsat 5
1998	22/12/1998	Landsat 5
1999	14/10/1999	Landsat 7
2000	30/09/2000	Landsat 7
2001	17/09/2001	Landsat 7
2002	20/09/2002	Landsat 7
2003	2/11/2003	Landsat 5
2004	19/10/2004	Landsat 5
2005	15/05/2005	Landsat 5
2006	2/05/2006	Landsat 5
2007	5/05/2007	Landsat 5
2008	12/09/2008	Landsat 5
2009	30/08/2009	Landsat 5
2010	13/05/2010	Landsat 5
2011	5/09/2011	Landsat 5
2012	1/10/2012	Landsat 5
2013	9/08/2013	Landsat 8
2014	28/08/2014	Landsat 8
2015	16/09/2015	Landsat 8
2016	4/10/2016	Landsat 8
2017	24/11/2017	Landsat 8
2018	13/12/2018	Landsat 8
2019	14/11/2019	Landsat 8

Image dates for 105/79

1994	18/11/1994	Landsat 5
1995	5/11/1995	Landsat 5
1996	23/11/1996	Landsat 5
1997	28/12/1997	Landsat 5
1998	13/11/1998	Landsat 5
1999	26/11/1999	Landsat 7
2000	9/10/2000	Landsat 7
2001	9/08/2001	Landsat 7
2002	29/09/2002	Landsat 7
2003	24/09/2003	Landsat 5
2004	13/11/2004	Landsat 5
2005	25/06/2005	Landsat 5
2006	11/05/2006	Landsat 5
2007	18/08/2007	Landsat 5
2008	21/09/2008	Landsat 5
2009	8/09/2009	Landsat 5
2010	27/09/2010	Landsat 5
2011	14/09/2011	Landsat 5
2012	24/09/2012	Landsat 5
2013	19/09/2013	Landsat 8
2014	5/08/2014	Landsat 8
2015	25/09/2015	Landsat 8
2016	27/09/2016	Landsat 8
2017	17/11/2017	Landsat 8
2018	6/12/2018	Landsat 8
2019	7/11/2019	Landsat 8

Image dates for 105/80

1994	2/11/1994	Landsat 5
1995	5/11/1995	Landsat 5
1996	23/11/1996	Landsat 5
1997	28/12/1997	Landsat 5
1998	13/11/1998	Landsat 5
1999	26/12/1999	Landsat 7
2000	9/10/2000	Landsat 7
2001	28/10/2001	Landsat 7
2002	29/09/2002	Landsat 7
2003	24/09/2003	Landsat 5
2004	13/11/2004	Landsat 5
2005	25/06/2005	Landsat 5
2006	25/04/2006	Landsat 5
2007	18/08/2007	Landsat 5
2008	21/09/2008	Landsat 5
2009	8/09/2009	Landsat 5
2010	30/11/2010	Landsat 5
2011	14/09/2011	Landsat 5
2012	26/10/2012	Landsat 5
2013	19/09/2013	Landsat 8
2014	5/08/2014	Landsat 8
2015	25/09/2015	Landsat 8
2016	27/09/2016	Landsat 8
2017	1/11/2017	Landsat 8
2018	6/12/2018	Landsat 8
2019	7/11/2019	Landsat 8

